cognizant of time and place. Her answers to questions were cogent. She could name objects and repeat sentences correctly, although her speech was slurred, slow-pitched, monotonous, and difficult. The tongue showed no atrophy nor fasciculation. Her facial expressions were fairly normal. Although there was no amyotrophy in the extremities, muscle tone was spastic, especially in the lower extremities. Jaw jerk and tendon reflex were exaggerated. Pathological grasping reflex, Hoffman reflex and Trömner reflex were induced bilaterally. Planter reflex was flexor bilaterally. No cerebellar ataxia was observed. As is mentioned later, her writing errors were, however, of great interest. She was not conscious of her illness and scored 7/18 on the frontal assessment battery [4]. Hasegawa's dementia rating scale (revised) was 23/30, suggesting mild cognitive impairment (normal range is above 21/30) [5]. Routine laboratory data were all within normal limits including those for syphilis, anti-human T cell leukemia virus 1 antibody, thyroid function, vitamin B_{12} and folic acid. The cerebrospinal fluid examination was unremarkable. Needle electromyography performed on the tongue, diaphragm, and anterior tibial muscle revealed mild chronic denervation. Magnetic resonance images (MRI) of the head revealed atrophy of the anterior part of the temporal and frontal lobes, slightly predominant on the right. Single photon emission computed tomography (SPECT) images disclosed decreased uptake of tracer, bilaterally, in the frontal and temporal lobes. After discharge she was observed as an outpatient, but her mental condition and motor symptoms gradually deteriorated. About five months after discharge, gastrostomy was performed for severe dysphagia. At which time, she had tetraparesis and could not respond to the examiner's instructions. She was transferred to the nursing hospital. Tracheostomy was not performed, and artificial ventilation not administered at the request of her family. The total duration of her illness was 18 months and she died of sudden respiratory failure.

3. Analysis of language function

Japanese language uses two distinct writing systems: kana characters, composed of simple phonograms with unambiguous phonetic readings, and kanji characters, a system of several thousand morphograms or ideograms.

On admission, her speech showed severe dysarthria and little intonation, and sounds and syllables were inconsistent. She occasionally had telegraphic speech and paraphrasia during spontaneous speech. The results of the WAB, examined during the first two weeks of admission, revealed spontaneous speech was non-fluent due to severe dysarthria. Repetition was mildly impaired. Although she could repeat nine words (each word was composed of two to ten characters) and two short sentences (each sentence was composed of eight and nine characters) without an error, she made two errors in repeating a long sentence composed of 20 characters, i.e. "新しい甘酒を五本のひょうたんに入れなさい" (Put fresh sweat alcohol into five gourds, in English). Object naming was mildly impaired (18/20), however, she could name all objects given phonemic cues. Sentence completion and responses in conversation were slightly impaired (8/10 and 8/10, respectively). As shown in Yes/No questions (60/60) and auditory word recognition (59/60), comprehension was not impaired.

In contrast to the results described above, her writhing was severely impaired. Although writing speed was slow, her formation of written characters showed no distortion. She made five errors in writing the same sentence as used in repetition: "新しい甘酒を五本のひょうたんに入れなさい" (she made two errors in repetition). She made four errors during writing six kanji words (each word was composed of two kanji characters), two errors in six kana words (each word was composed of three or four kana characters), and thirteen errors in four sentences (each sentence was composed of nine or ten characters). Most of the errors were omission of kana characters and adjuncts, such as postpositional particles. For example: "山上１本立て居す" instead of "山の上に木が１本立って居ます". The sentence is written, as normal, using a mixture of kanji and kana, and an English translation is: "There is a tree on the mountain". "の" and "に" are both particles, written in kana letters. And "木が" is the subject of the sentence, composed of "木"("tree") and "が"(a postpositional particle). "ま" is one of the so-called "okurigana", or kana characters added after kanji to indicate inflection. Other types of errors were substitution or addition of letters. Her ability to copy both letters and sentences was unimpaired. She could copy the sentence "新しい甘酒を五本のひょうたんに入れなさい" without an error.

After about three months, during follow up at the outpatient clinic, perseverative errors and paragraphia emerged. Moreover, morphology of her written characters became slightly distorted.

When tube feeding was necessary, she was no longer able to hold writing implements.

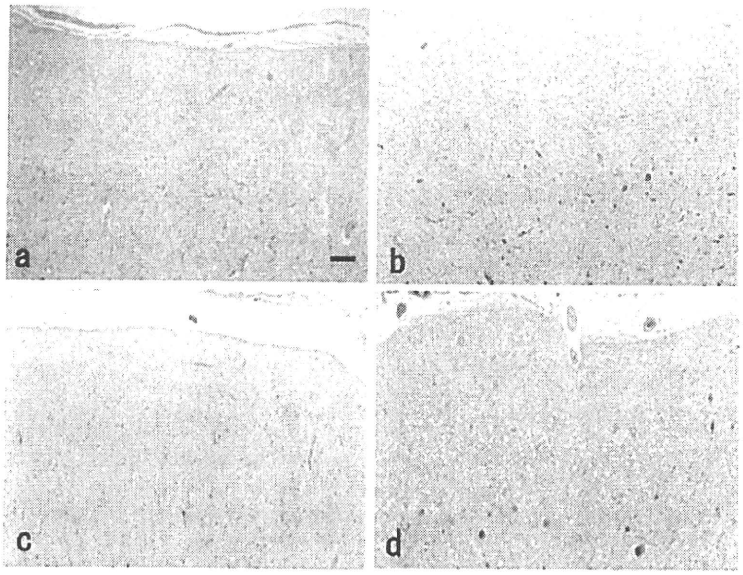

Fig. 1. Superficial spongiosis of the left frontal lobe cortices. a: superior frontal gyrus, b: middle frontal gyrus, c: inferior frontal gyrus, d: precentral gyrus. Severe spongiosis in the middle frontal (b) and precentral (d) gyri are shown. HE stain. Scale bar = 400 μm. (Colours are visible in the online version of the article; http://dx.doi.org/10.3233/BEN-2010-0276)

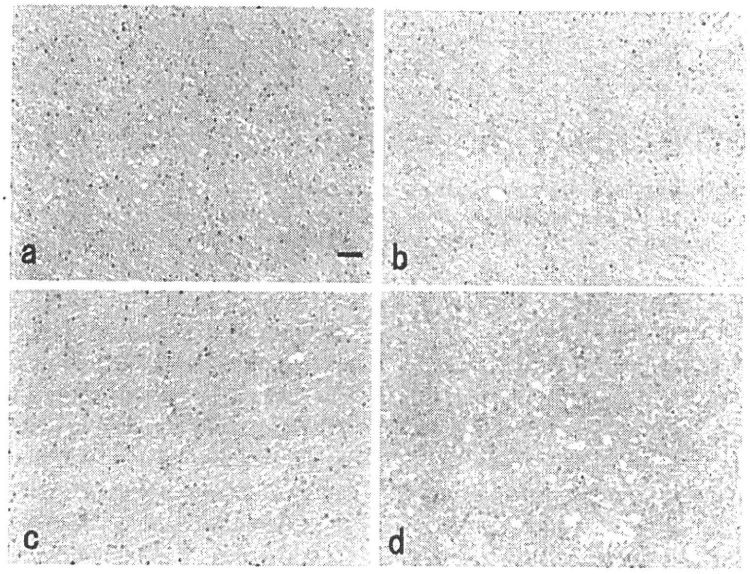

Fig. 2. Subcortical white matter of the left frontal lobe. a: superior frontal gyrus, b: middle frontal gyrus, c: inferior frontal gyrus, d: precentral gyrus. Numerous macrophages are observed in the middle frontal (b) and precentral (d) gyri. HE stain. Scale bar = 200 μm. (Colours are visible in the online version of the article; http://dx.doi.org/10.3233/BEN-2010-0276)

4. Neuropathological findings

General pathological examination revealed severe thinning of the diaphragma.

The brain weighed 1060 g prior to fixation. Macroscopic examination revealed circumscribed atrophy of the anterior temporal and frontal lobes bilaterally. Both lateral ventricles were slightly dilated. The substantia nigra was significantly depigmented.

Sections of paraffin-embedded tissue were stained with hematoxylin and eosin (H & E), Klüver-Barrera, and Bodian stains. In addition, immunohistochemistry for selected areas was performed using anti-ubiquitin (Dako; Japan; 1:100), anti-tau (AT8; Innunogenetics;

Table 1
Summary of lesion distribution

lesion (gyrus)	neuronal loss	superficial spongiosis	macrophage invasion	TDP pathology
superior frontal	mild	moderate	none	mild
middle frontal	mild	severe	severe	moderate
inferior frontal	mild	mild	none	mild
precentral	severe	severe	severe	moderate

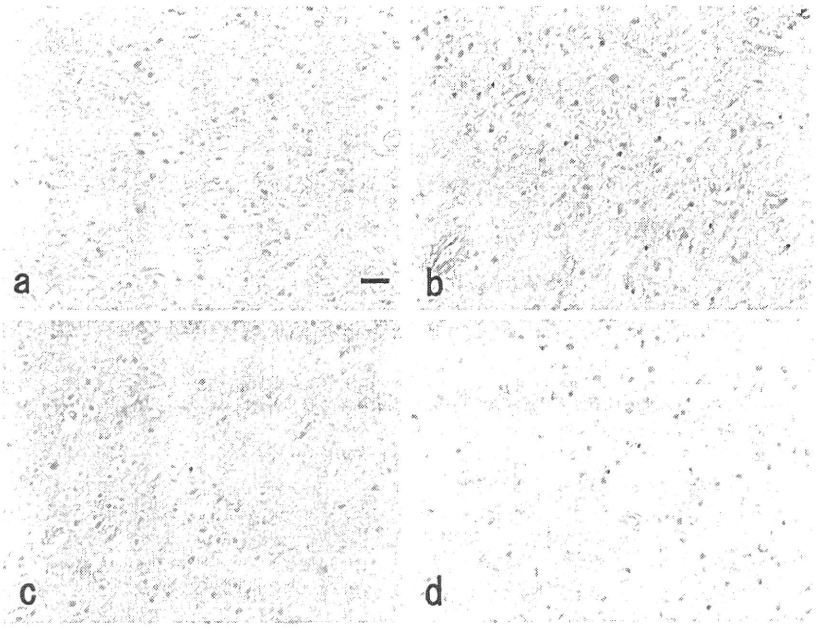

Fig. 3. Neuronal intra-cytoplasmic inclusions in the cortical neurons. a: superior frontal gyrus, b: middle frontal gyrus, c: inferior frontal gyrus, d: precentral gyrus. Numerous inclusions can be seen in the middle frontal (b) and precentral (d) gyri. Anti-phosphorylated-TDP-43-immunostain. Scale bar = 80 μm. (Colours are visible in the online version of the article; http://dx.doi.org/10.3233/BEN-2010-0276)

1:1000), and anti-phosphorylated-TDP-43 (p403/404, Cosmo Bio; California; 1:1000) antibodies.

Superficial spongiosis, neuronal loss, gliosis and rarefaction of the neuropil were observed in the frontal and temporal lobe cortices, especially in the precentral gyrus and posterior part of the middle frontal gyrus bilaterally (Fig. 1). Superficial spongiosis was also observed in the other frontal cortex, but to a lesser degree. Plenty of macrophages were observed in the subcortical white matter of these areas (Fig. 2). There were several clusters of macrophages in the deeper cortical layer of the precentral gyrus, indicating loss of Betz cells. Moderate neuronal loss was observed in the transitional area between CA1 and subiculum. Only a few neurofibrillary tangles were observed in the parahippocampal gyrus. No pathological change was observed in the left parietal and occipital lobes.

The pyramidal tracts showed almost complete axonal loss in the bilateral cerebral peduncles and pyramids. Neurons in the hypoglossal and ambiguous nuclei were preserved in number, however a few Bunina bodies were observed in the remaining neurons. The substantia nigra showed severe neuronal loss and gliosis with no Lewy bodies. The locus ceruleus showed mild neuronal loss and two Lewy bodies. The cerebellum was unremarkable. There were no neurofibrillary tangles in the brainstem or cerebellum.

In the spinal cord, moderate to severe loss of anterior horn cells and several Bunina bodies in the remaining neurons were observed. The pyramidal tracts showed almost complete axonal loss in the lateral columns. The posterior columns were unremarkable. Neurons in Onuf's nucleus were preserved in number.

Immuno-histochemistry showed ubiqutin and TDP-43-positive and tau-negative neuronal intracytoplasmic inclusions in the hipocampal dentate gyrus and frontal lobe cortex (Fig. 3). We detected these inclusions in the middle frontal and precentral gyri much more than in other frontal lobe cortices. Only a small number of TDP-43 positive dystrophic neurites were observed.

TDP-43 positive neuronal intranuclear inclusions and glial cells were not observed.

Summary of the pathological changes including immunohistochemistry are shown in Table 1.

5. Discussion

The presented case features a combination of progressive pseudobulbar palsy, frontal lobe type dementia, pyramidal tract signs and progressive amyotrophy. MRI revealed atrophy of the frontal and temporal lobes. Decreased blood flow in the frontal and temporal lobes was demonstrated by SPECT images. Pathological features of the case are: degeneration of both upper and lower motor neurons, degeneration of frontal and temporal lobes, Bunina bodies of the remaining lower motor neurons and TDP-43 pathology. These features are fully compatible with the diagnosis of ALS-D.

In progressive nonfluent aphasia, agraphia with effortful writing containing spelling error and agrammatism may be observed [6]. Agrammatism refers to omission or incorrect use of grammatical terms, including articles, prepositions, auxiliary verbs, inflexions, and derivations. From an initial stage, the presented patient showed progressive speech output disorder due to pseudobulbar palsy. Although telegraphic speech and occasional paraphasia were observed, frequency of such errors was quite less than that of writing errors. As shown in the WAB result, comprehension, naming and repetition were almost preserved when obvious agraphia was observed. Therefore, we believe the agraphia observed in our case did not derive from aphasia. Although perseverative errors were observed at a late stage, this can be attributed to frontal lobe dysfunction.

Omission of kana letters in Japanese and related syntactic errors in English have been reported in ALS with or without dementia [2,3,7,8]. The writing errors observed in our case concur well with previous descriptions. Although the lesion associated with pure agraphia is thought to be in the left frontal or parietal lobe [9], detailed clinicopathological analysis of ALS is unreported. A single autopsied case from the United States suggests that the left frontal or parietal lobe may be linked with the lesion responsible for syntactic errors in writing [7]. However, pathological findings related to agraphia were not described.

Our case reveals a left frontal lobe lesion with emphasis on the caudal part of the middle frontal gyrus, combined with immuno-histochemistry and other ALS-related indicators. Frontal and temporal lobe lesions including the hippocampal dentate gyrus have already been associated with dementia symptom in ALS-D [1]. A detailed description of each neuropsychological symptom and lesion remains to be elucidated, however.

The posterior part of the left middle frontal gyrus (Exner's area) is thought to play a pivotal role in writing letters and lesions there to cause agraphia [10,11]. Only a small number of cases of pure agraphia due to circumscribed lesions in Exner's area have been reported thus far [12–15]. Reports from Japan reveal phonological errors such as omission and paragraphia of kana letters associated with Exner's area lesion in cerebrovascular disease [15–17]. These errors concur well with the writing disorders observed in our case.

In the case described here, lesion distribution in the left frontal lobe was concentrated in Exner's area and no pathological change was observed in the left parietal lobe, which is another lesion associated with agraphia. We believe this is the first report that links clinicopathology in progressive agraphia without aphasia and detailed pathological examination including immunohistochemistry. Of course, further accumulation of clinicopathological examination focusing ALS-D and agraphia would be required to clarify our hypothesis.

Acknowledgements

This study was supported by a grant from the Tamagawa University Center of Excellence from the Ministry of Education, Culture, Sports, Science and Technology (MEXT) and the Core Research for Evolutionary Science and Technology (CREST; No. 17022035) and by a Grant-in-Aid for Scientific Research on Priority Areas–System Study on Higher-order Brain Functions from MEXT (No. 20020026). This study was also supported in part by a Showa University Grant-in-Aid for Innovative Collaborative Research Projects and a Special Research Grant-in-Aid for Development of Characteristic Education from MEXT.

References

[1] I.R.A. Mackenzie, The neuropathology of FTD associated with ALS, *Alzheimer Dis Assoc Disord* 4 (2007), S44–S49.

[2] H. Ichikawa, S. Koyama, H. Ohno, K. Ishihara, K. Nagumo and M. Kawamura, Writing errors and anosognosia in amyotrophic lateral sclerosis with dementia, *Behav Neurol* **19** (2008), 107–116.

[3] M. Kanzaki, M. Sato, G. Ogawa, N. Miyamoto, K. Motoyoshi, K. Kamakura and K. Takeda, A case of dementia with motor neuron disease associated with agraphia – the omission of kana letters–, *Clin Neurol* **44** (2004), 673–676 (in Japanese with English abstract).

[4] B. Dubois, A. Slachevsky, I. Litvan and B. Pillon, The FAB: a Frontal Assessment Battery at bedside, *Neurology* **55** (2000), 1621–1626.

[5] T. Hosokawa, Y. Yamada, A. Isagoda and R. Nakamura, Psychometric equivalence of the Hasegawa Dementia Scale-Revised with the Mini-Mental State Examination in stroke patients, *Perceptual and Motor Skills* **79** (1994), 664–666.

[6] D. Neary, J.S. Snowden, L. Gustafson, U. Passant, D. Stuss, S. Black, M. Freedman, A. Kertesz, P.H. Robert, M. Albert, K. Boone, B.L. Miller, J. Cummings and D.F. Benson, Frontotemporal lobar degeneration. A consensus on clinical diagnostic criteria, *Neuroloy* **51** (1998), 1546–1554.

[7] J.H. Ferguson and F. Boller, A different form of agraphia: Syntactic writing errors in patients with motor speech and movement disorders, *Brain Lang* **4** (1977), 382–389.

[8] M. Satoh, K. Takeda and S. Kuzuhara, Agraphia in intellectually normal Japanese patients with ALS: omission of kana letters, *J Neurol* **256** (2009), 1455–1460.

[9] P. Marcie and H. Hécan, Agraphia: writing disorders associated with unilateral cortical lesions, in: *Clinical Neuropsychology*, K.N. Heilman and E. Valenstine, eds, Oxford University Press, New York and Oxford, 1979, pp. 92–127.

[10] S. Exner, *Unterschingen über die Localisation der Functionen in der Grösshirnrinde des Menschen,* W. Braumuller, Wien, 1881.

[11] J.M. Nielsen, *Agnosia, Apraxia, Aphasia. Their value in cerebral localization*, P.B. Hoeber, New York, 1946.

[12] H.C. Gordinier, A case of brain tumor at the base of the second left frontal convolution, *Am J Med Sci* **117** (1899), 526–535.

[13] G. Aimard, M. Devic, M. Lebel, P. Trouillas and D. Boisson, *Agraphie pure (dynamique?) d'origine frontale. A propos d'un observation*, *Rev Neurol* **131** (1975), 505–512.

[14] S.W. Anderson, A.R. Damasio and H. Damasio, Troubled letters but not numbers. Domain specific cognitive impairment following focal damage in frontal cortex, *Brain* **113** (1990), 749–766.

[15] K. Abe, R. Yokoyama, S. Yorifuji and T. Yanagihara, A jargon agraphia and selective agraphia of Kana resulting from an infarct in the left middle frontal gyrus, *Jpn J Neuropsychol* **9** (1993), 196–201 (in Japanese with English abstract).

[16] H. Tohgi, K. Saitoh, S. Takahashi, H. Takahashi, K. Utsugisawa, H. Yonezawa, K. Hatano and T. Sasaki, Agraphia and acalculia after a left prefrontal (F1, F2) infarction, *J Neurol Neurosurg Psychiatry* **58** (1995), 629–632.

[17] Y. Sakurai, K. Matsumura, T. Iwatsubo and T. Momose, Frontal pure agraphia for kanji or kana: Dissociation between morphology and phonology, *Neurology* **49** (1997), 946–952.

Journal of the Neurological Sciences 294 (2010) 95–101

Contents lists available at ScienceDirect

Journal of the Neurological Sciences

journal homepage: www.elsevier.com/locate/jns

Neuronal NOS is dislocated during muscle atrophy in amyotrophic lateral sclerosis

Naoki Suzuki [a,*], Hideki Mizuno [a], Hitoshi Warita [a], Shin'ichi Takeda [b], Yasuto Itoyama [a], Masashi Aoki [a]

[a] Department of Neurology, Tohoku University School of Medicine, 1-1 Seiryo-machi, Aoba-ku, Sendai 980-8574, Japan
[b] Department of Molecular Therapy, National Institute of Neuroscience, National Center of Neurology and Psychiatry, Kodaira, Tokyo 187-8502, Japan

ARTICLE INFO

Article history:
Received 1 September 2009
Received in revised form 23 March 2010
Accepted 23 March 2010

Keywords:
Amyotrophic lateral sclerosis (ALS)
Motor neuron disease (MND)
Muscle atrophy
Neuronal nitric oxide synthase (nNOS)
Superoxide dismutase (SOD1)

ABSTRACT

Previously, we demonstrated that neuronal nitric oxide synthase (nNOS) is activated and promotes muscle atrophy in skeletal muscle during tail suspension, a model of unloading and denervation. Here, we examined patients with amyotrophic lateral sclerosis (ALS) and mutant (H46R) SOD1 transgenic (Tg) mice model using immunohistochemistry, Western blotting and real time PCR. We found cytoplasmic nNOS staining of angulated muscle fibers in patients with ALS. We also examined mutant SOD1 Tg mice and found cytoplasmic nNOS staining even before the onset of clinical muscle atrophy. In the Tg mice, nNOS was largely extracted with 100 mM NaCl and barely detected in the pellet fraction, suggesting fragile anchoring of nNOS to the sarcolemma. We also showed an elevated expression of atrogin-1, key molecules in muscle atrophy at the end stage. A common nNOS dislocation/atrogin-1/muscle atrophy pathway among tail suspension, denervation and ALS is suggested. nNOS modulation therapy may be beneficial in several types of muscle atrophy.

1. Introduction

Amyotrophic lateral sclerosis (ALS) is a fatal neurodegenerative disease caused by the selective death of motor neurons [1–3]. Approximately 10% of the cases of ALS are inherited, usually as an autosomal dominant trait. In 25% of familial cases, the disease is caused by mutations in the gene encoding cytosolic copper–zinc superoxide dismutase (SOD1) [4–6]. The reason why the motor neuron is selectively damaged has not been elucidated. Additionally, the mechanism of muscle atrophy followed by motor neuron death has not been resolved. The overexpression of mutant human SOD1 in mice is used as a model of ALS. These mutant SOD1 transgenic (Tg) mice reproduce the major phenotypic features of human ALS [7,8], and could be used in analyzing the pathomechanism of ALS [9,10].

Reduced muscle activity such as bed rest, limb immobilization, denervation, or unloading (e.g. tail suspension or space flight) leads to significant muscle atrophy [11,12]. In these conditions, the atrophying muscles show increased rates of protein degradation mainly through the activation of the ubiquitin proteasome system [13,14], and the muscle-specific E3 ubiquitin ligases, Muscle-specific RING finger protein 1 (MuRF-1) and atrogin-1/Muscle atrophy F-box protein (MAFbx), are commonly up-regulated [13,14]. Recent studies further showed that muscle inactivity results in the suppression of the IGF-1/PI3k/Akt pathway [15–18] and activation of transcription factors such as the Foxo family and NFκB [19–21].

Several molecules are proposed as a mechanical sensor or a trigger of disuse atrophy. It has been reported that muscles from tumor-bearing mice exhibited reduced levels of dystrophin, the protein that is mutated in Duchenne muscular dystrophy, together with a reduction of dystrophin-associated glycoprotein [22,23]. These results raise the possibility that the dystrophin glycoprotein complex (DGC) works as a regulator of muscle atrophy or serves as a scaffold for anti-atrophic signal transduction.

Recently, we examined the expression and function of the members of DGC in skeletal muscle during tail suspension, a model of unloading, and demonstrated that neuronal nitric oxide synthase (nNOS), a member of DGC, is activated in unloading conditions and promotes muscle atrophy [24]. We also showed that a nNOS-specific inhibitor significantly attenuates suspension-induced muscle atrophy. Furthermore, we showed the involvement of nNOS in the denervation-induced muscle atrophy process. Thus, nNOS and nitric oxide (NO) are new therapeutic targets for disuse-induced muscle atrophy.

We hypothesized that the same phenomena exist under the pathomechanism of ALS. For the purpose of examining the pathomechanism of muscle atrophy in ALS, here we examined muscles from patients with ALS and a mouse model of ALS. We found nNOS dislocation during the disease process of mutant SOD1 Tg mice. A common nNOS dislocation/atrogin-1 pathway for tail suspension, denervation and ALS induced muscle atrophy is suggested.

Abbreviations: ALS, amyotrophic lateral sclerosis; DGC, dystrophin glycoprotein complex; eNOS, endothelial nitric oxide synthase; Gc, gastrocnemius; H46R, histidine to arginine at position 46; iNOS, inducible nitric oxide synthase; MAFbx, Muscle atrophy F-box protein; MuRF-1, Muscle-specific RING finger protein 1; nNOS, neuronal nitric oxide synthase; NO, nitric oxide; SOD1, superoxide dismutase 1; TA, tibialis anterior; Tg, transgenic.

* Corresponding author. Tel.: +81 22 717 7189; fax: +81 22 717 7192.
E-mail address: naoki@em.neurol.med.tohoku.ac.jp (N. Suzuki).

0022-510X/$ – see front matter © 2010 Elsevier B.V. All rights reserved.
doi:10.1016/j.jns.2010.03.022

Table 1
Patients list. Characteristics and immunostaining results of patients with ALS and normal control. ALS, amyotrophic lateral sclerosis; BB, biceps brachii; RF, rectus femoris; TA, tibialis anterior; M, male; F, female.

No.	Sex	Age	Disease	Months after onset	nNOS membrane	nNOS cytosol	α1-syntrophin	Site of biopsy
1	M	71	ALS	4	+	+	+	BB
2	F	58	ALS	7	+	−	+	BB
3	M	47	ALS	8	+	+	+	TB
4	F	55	ALS	8	+	+	+	BB
5	M	45	ALS	13	+	+	+	TA
6	M	67	ALS	20	+	−	+	RF
7	M	70	ALS	30	+	+	+	TA
8	F	68	ALS	48	+	−	+	TA
9	F	47	ALS	144	+	+	+	BB
10	M	46	ALS	300	+	+	+	BB
11	M	19	Normal	–	+	−	+	BB
12	F	59	Normal	–	+	−	+	BB
13	M	29	Normal	–	+	−	+	BB

2. Methods

2.1. Patients

We studied skeletal muscle biopsies obtained from 10 patients who had, according to the El Escorial criteria, a diagnosis of definite ALS at the Department of Neurology, Tohoku University School of Medicine. No patients had a family history of motor neuron disease. The patients were 6 males and 4 females, with the age at the time of muscle biopsy between 45 and 71 years, as shown in Table 1. At the time of biopsy, the duration of disease was 4–300 months. Muscle biopsy was performed with each patient's written informed consent. The routine histochemical analysis of all biopsies showed neurogenic changes ranging from mild to severe. We used 3 normal patients as positive controls and Becker type muscular dystrophy diagnostic muscle biopsies as negative controls for nNOS staining.

2.2. The clinical course of H46R SOD1 transgenic mice

Transgenic (Tg) mice expressing H46R mutant human SOD1 were generated as described previously [7,8,25–28]. The Tg mice developed motor neuron disease with a mean age of onset in clinical weakness of approximately 21 weeks. In each Tg mouse we carefully observed the development of the symptoms of ALS. Clinically apparent weakness, indicated by dragging of one hindlimb without limb tremor, was evident somewhat later. Simultaneously with the onset of clinical weakness, the affected mice showed prominent muscle atrophy and weight loss. While the initial clinical manifestation of weakness was unilateral leg paralysis, this progressed and became bilateral in the Tg mice. In the early stages of the illness, another distinctive abnormality

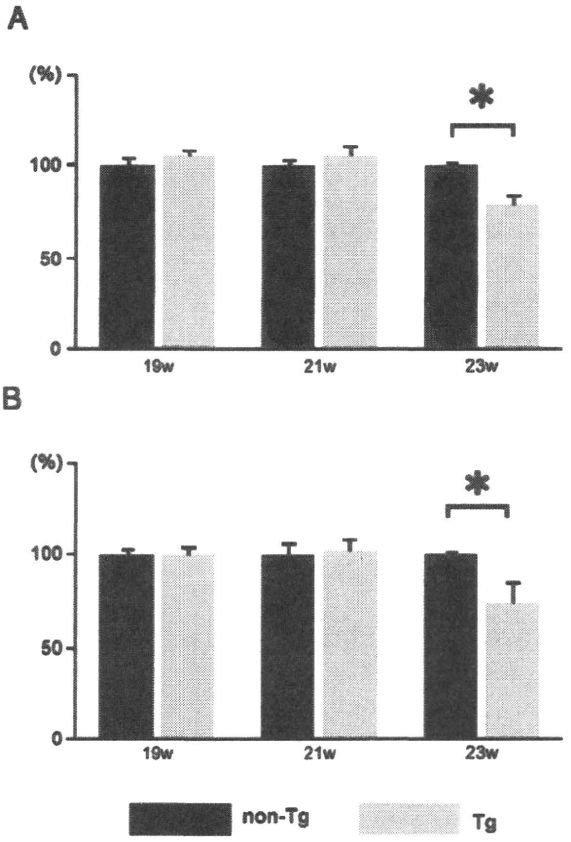

Fig. 2. Muscle weight during the disease course of mutant SOD1 Tg mice. Weights of TA (A) and Gc (B) muscles from Tg and non-Tg mice are normalized to body weight, and are expressed as percentage of non-Tg mice of each age ($n=5$ for each group). Student's t-test, $^{*}p<0.05$.

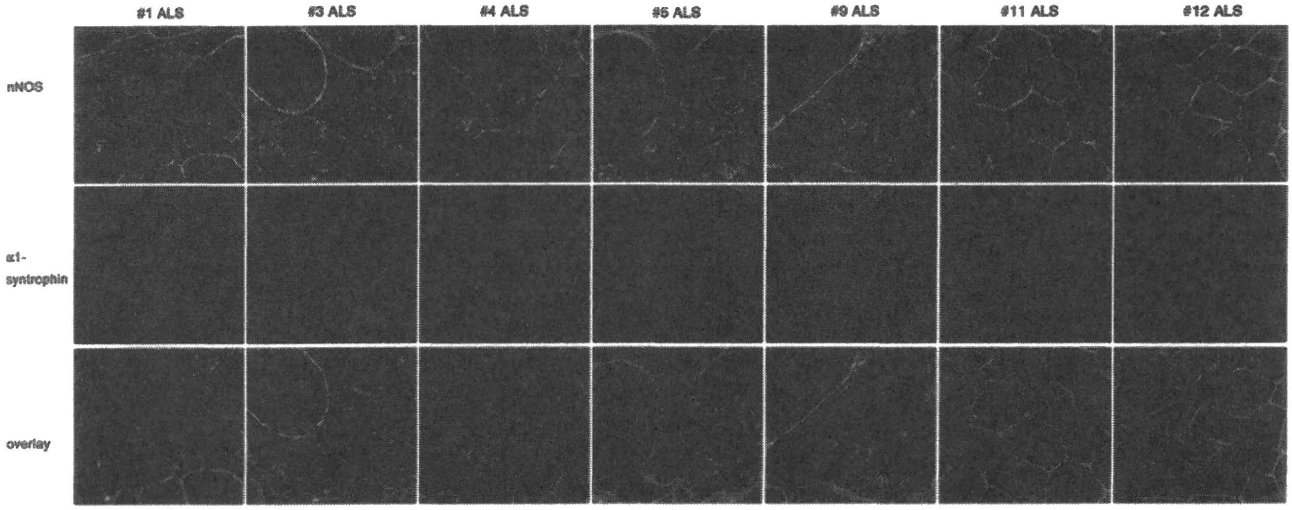

Fig. 1. Dislocation of nNOS is observed in patients with ALS. nNOS in normal and affected muscles was stained with nNOS and α1-syntrophin antibodies. Overlay image is also presented. Scale bar, 50 μm.

was the increased tone in the tail musculature, resulting in an elevated, segmentally spastic tail posture. At end stage, the affected mice could not drink water and died. The mean age at death from the disease was around 24 weeks. The animals were allowed ad libitum access to food and drinking water. The animals were sacrificed by cervical dislocation, and the tibialis anterior (TA) and gastrocnemius (Gc) muscles were excised for analysis. All experimental protocols and procedures were approved by the Animal Committee of the Tohoku University School of Medicine, Japan.

2.3. Tissue preparation from Tg mice

Body and wet muscle were weighed. The TA and Gc muscles were collected individually using standard dissection methods and cleaned of excess fat, connective tissue, and tendons. Several of the muscles were frozen in isopentane cooled by liquid nitrogen for histological and immunohistochemical analysis, and the other muscles were frozen directly in liquid nitrogen for RNA isolation or protein extraction and stored at −80 °C.

2.4. Real time PCR

Total RNA was isolated using TRIzol (Invitrogen, Carlsbad, CA). For real time PCR, first strand cDNA was synthesized using oligo-dT primers. The expression levels of selected genes (nNOS, MuRF-1, atrogin-1/MAFbx and β-actin) were analyzed using LightCycler (Roche, Basel, Switzerland) following the manufacturer's instructions.

2.5. Immunohistochemistry

Cryostat sections of muscle tissue (10 μm thick) cut in the middle part of the TA muscle belly to obtain the largest myofiber diameter, were placed on poly-L-lysine-coated slides, air dried, and, post-fixed in acetone at −20 °C and pre-incubated in phosphate-buffered saline (PBS) containing 5% goat serum and 1% bovine serum albumin for 30 min at room temperature. Polyclonal anti-nNOS (Invitrogen) and anti-α1-syntrophin (Biogenesis, Poole, UK) were applied overnight at 4 °C. Following incubations with the appropriate secondary antibodies, mounted sections were observed by using an Olympus confocal microscope (Tokyo, Japan). nNOS dislocated fibers per 100 muscle fibers were counted in mutant SOD1 Tg mice and control mice.

2.6. Western blotting

Total skeletal muscle protein was extracted from mouse Gc muscle for Western blot analysis. We used the Bradford method to determine the protein concentrations. Then, protein fractions were extracted with a reducing sample buffer containing 2.3% SDS, 70 mM Tris–HCl, 5% β-mercaptoethanol and Complete inhibitor cocktail (Roche). Protein (30 μg per lane) was separated on a 10–20% gradient SDS-polyacrylamide gel. The resulting gel was subsequently transferred to

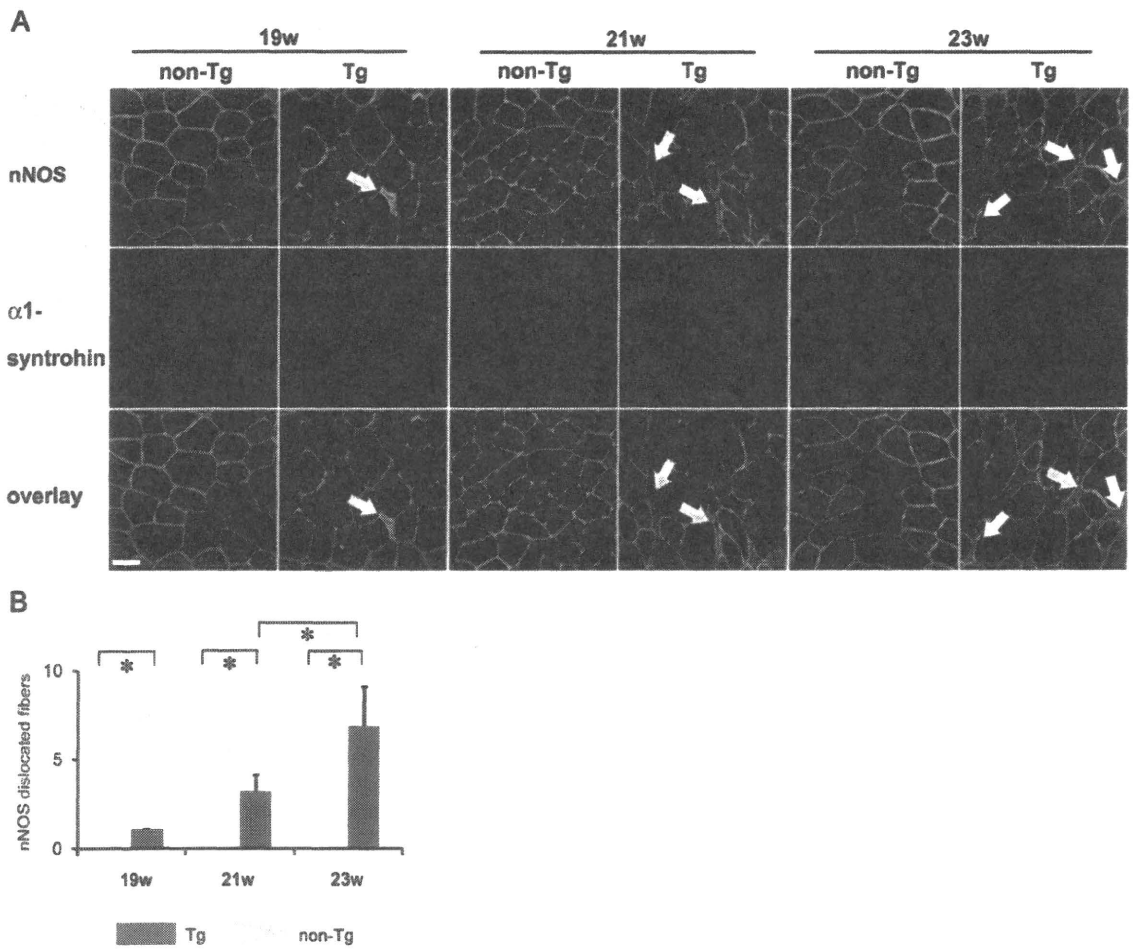

Fig. 3. Localization of nNOS during the disease course of mutant SOD1 Tg mice. (A) Transverse muscle sections from 19 weeks (w), 21 w, 23 w Tg and non-Tg mice were stained with anti-nNOS and α1-syntrophin antibodies. An overlay image is also presented. Scale bar, 50 μm. Arrows represent the nNOS dislocated angulated fibers. (B) nNOS dislocated fibers per 100 muscle fibers were counted in mutant SOD1 Tg mice and control mice. ($n = 5$ for each group). Student's t-test, $^*p < 0.05$.

a polyvinylidene difluoride membrane (Millipore, Billerica, MA) using 242 mA for 1 h. The blot was later incubated with primary antibodies. The signals were detected using the enhanced chemiluminescence method (GE Healthcare, Piscataway, NJ). The following antibodies were used for immunoblotting: anti-α1-syntrophin, anti-aquaporin-4 (Chemicon, Billerica, MA), anti-caveolin-3, α-sarcoglycan, β1-sarcoglycan, dystrobrevin (Novocastra, Newcastle upon Tyne, UK), anti-nNOS (BD Biosciences, Franklin Lakes, NJ), GAPDH, inducible NOS (iNOS) (Santa Cruz Biotechnology, Santa Cruz, CA), and endothelial NOS (eNOS) (Cayman Chemicals, Ann Arbor, MI) antibodies. The bands were quantified in densitometry using Image-J [24].

2.7. Subcellular fractionation

The subcellular fractionation was performed according to the method described by Brenman et al. [29] and described previously [24]. Briefly, the Gc muscle was homogenized in 10 volumes (w/v) of buffer A (25 mM Tris–HCl, pH 7.4, 100 mM NaCl, 1 mM EDTA, 1 mM EGTA). The nuclei of the muscle were pelleted by centrifugation at 1000×g. The supernatant was then centrifuged at 20,000×g to yield supernatant S1. The resulting heavy microsomal pellet was resuspended in buffer B (500 mM NaCl added to buffer A), incubated for 30 min at 4 °C with agitation, and centrifuged at 15,000×g, yielding supernatant S2. The pellet from this last centrifugation was resuspended in buffer B containing 0.5% Triton X-100, incubated for 30 min at 4 °C with agitation, and centrifuged at 15,000×g to create supernatant S3 and the final pellet, P. The fractions were resolved using the sample buffer and analyzed by SDS-polyacrylamide gel electrophoresis. The bands are quantified in densitometry.

2.8. Statistical analysis

Statistical differences were determined by either Student's unpaired *t*-test or the Mann–Whitney test. All data are expressed as means ± s.e.m. Statistical significance was defined as $p<0.05$ (asterisk).

3. Results

3.1. Dislocated nNOS is observed in human ALS patients

Previously, we demonstrated that neuronal nitric oxide synthase (nNOS) is activated and promotes muscle atrophy in skeletal muscle during tail suspension, a model of unloading and denervation. To examine whether nNOS is involved in the pathomechanism of ALS, we first stained biopsied human skeletal muscle samples of ALS patients with nNOS and α1-syntrophin (Table 1 and Fig. 1). These patients were all sporadic cases. In the muscle of control patients nNOS was localized only at the sarcolemma. The nNOS staining patterns were co-localized with α1-syntrophin. We found nNOS staining of the cytoplasm in some atrophied muscle fibers in ALS patients. Some nNOS dislocated fibers were abnormally small, round or hypertrophied muscle fibers. As a negative control of immunohistochemistry for nNOS, we used Becker type muscular dystrophy in which nNOS protein is not stained at the sarcolemma (data not shown). The nNOS dislocation would have no relation to the extent of muscle atrophy or disease duration in this small sample size due to the variation of the disease course in human ALS. These results prompted us to study the role of dislocated nNOS during the disease course of the mutant SOD1 Tg mice.

3.2. Dislocated nNOS is observed before the onset of muscle atrophy in Tg mice

To elucidate the molecular mechanisms of muscle atrophy in ALS, female H46R mutant SOD1 Tg mice [8,25] were divided into 3 groups (8 mice each): pre-symptomatic (aged 19 weeks), onset (aged 21 weeks, just after onset) and end stage (aged 23 weeks); and examined with age-matched non-Tg littermate controls. The weight of the TA and Gc muscles/body weight was decreased to ~80% of the control mice at the end stage in this mice model (Fig. 2).

The immunohistochemical expression patterns of the components of DGC, dystrophin, laminin-α2, α1-syntrophin, and caveolin-3 were not changed during the disease course (Fig. 3 and data not shown). Importantly, immunohistochemistry revealed that nNOS was dislocated from the sarcolemma to the cytoplasm even before and at the onset of disease (Fig. 3). We also found increasing numbers of nNOS dislocated fibers as the disease progressed. The nNOS mRNA levels were not significantly reduced (data not shown), and total nNOS protein was not changed (Fig. 4A). Subcellular fractionation revealed a faint amount of nNOS in the P (pellet) fraction at the disease onset (Fig. 4B,C). Otherwise, S1 (soluble) fraction revealed no change in nNOS and α1-syntrophin. iNOS, another member of the NOS family, was significantly increased in the Tg mice (Fig. 5A,C). eNOS and other members of DGC (caveolin-3, α1-syntrophin, aquaporin-4, α, β-sarcoglycan and dystrobrevin) were not changed during the disease course (Fig. 5A–C). These results indicate that nNOS dislocates to the cytoplasm and iNOS is abnormally expressed during the disease course.

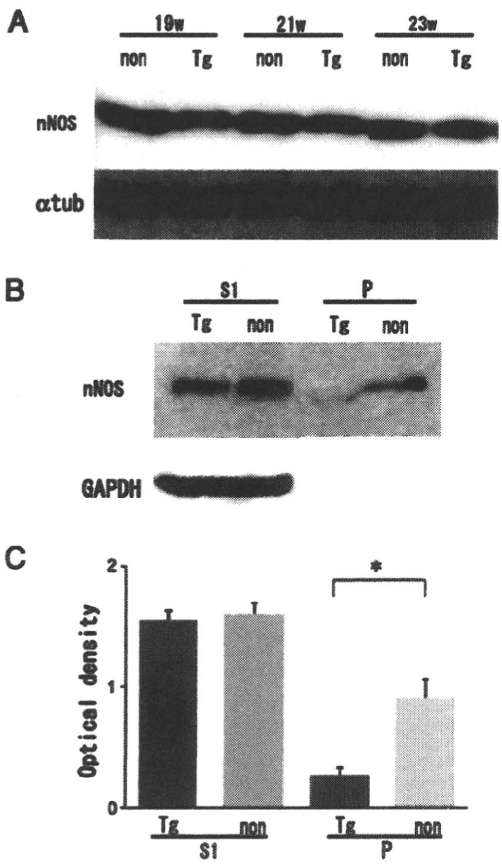

Fig. 4. Western blotting and subcellular fractionation of nNOS in mutant SOD1 Tg mice. (A) Immunoblots of mouse Gc muscle extracts for nNOS from 19 weeks (w), 21 w, 23 w Tg and non-Tg mice. All lanes contain 30 μg of total protein. The experiments were performed 3 times and representative pictures are presented. (B) Subcellular fractionation of Gc muscle extracts from 21 w Tg and non-Tg mice staining for nNOS and GAPDH. P indicates insoluble pellet after sequential extraction of skeletal muscle homogenates with 100 mM NaCl (S1), 500 mM NaCl, and 0.5% Triton X-100. Representative data are presented. (C) Quantification of nNOS signals in S1 and P fractions of muscle extracts shown in B ($n=4$/each group). Mann–Whitney test, $^*p<0.05$.

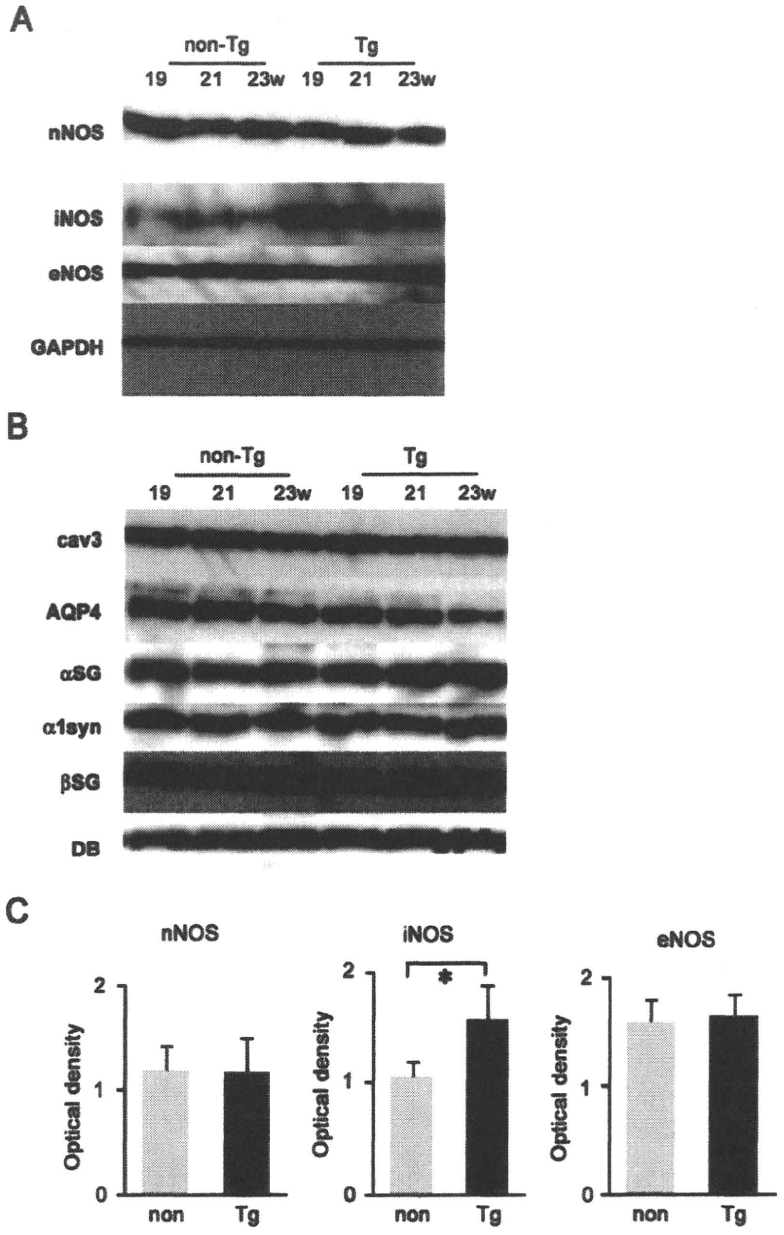

Fig. 5. Total amounts of proteins of NOS family and DGC components during the disease course in mutant SOD1 Tg mice. (A) Immunoblots of mouse Gc muscle extracts for NOS family and GAPDH from 19 weeks (w), 21 w, 23 w Tg and non-Tg mice. (B) Immunoblots of mouse Gc muscle extracts for DGC components from 21-week-old Tg and non-Tg mice. All lanes contain 30 μg of total protein. The experiments were performed 3 times and representative pictures are presented. αsyn, α1-syntrophin; AQP4, aquaporin-4; cav3, caveolin-3; αSG, α-sarcoglycan; βSG, β1-sarcoglycan; DB, dystrobrevin. (C) The amounts of nNOS, iNOS, and eNOS in Tg and non-Tg mice were quantified ($n=4$). Mann–Whitney test, $^{*}p<0.05$.

Previously, we reported that the dislocated nNOS produces excessive NO and ends in muscle atrophy during tail suspension [24]. Recently, several groups have pointed out that the ubiquitin proteasome pathway is largely involved in selective protein degradation during the muscle atrophy process [13,14,30]. In our previous study [24], we found no elevation of E3 ubiquitin ligases during tail suspension in nNOS-null muscle, although we found the elevation of E3 ubiquitin ligases in wild type muscle, suggesting up-regulations of E3 ubiquitin ligases were downstream events of nNOS dislocation in muscle atrophy. Consistent with this, the mRNA levels of the muscle-specific E3 ubiquitin ligase, atrogin-1/MAFbx (not MuRF1), were significantly increased in the mutant SOD1 Tg mice at the end stage (Fig. 6A,B).

4. Discussion

In our previous report, we demonstrated for the first time that nNOS is dislocated from the sarcolemma to the cytoplasm during tail suspension and denervation, whereas other members of DGC are normally expressed at the sarcolemma [24]. Here we demonstrated the dislocation of nNOS during the disease course of human ALS and a mouse model of ALS. The time point of nNOS dislocation was around the onset of the disease but before the apparent progression of muscle atrophy.

NO possesses both neuroprotective and neurodegenerative effects in the nervous system [31,32]. There are several reports on the relationship between ALS and nNOS, focusing especially on the spinal

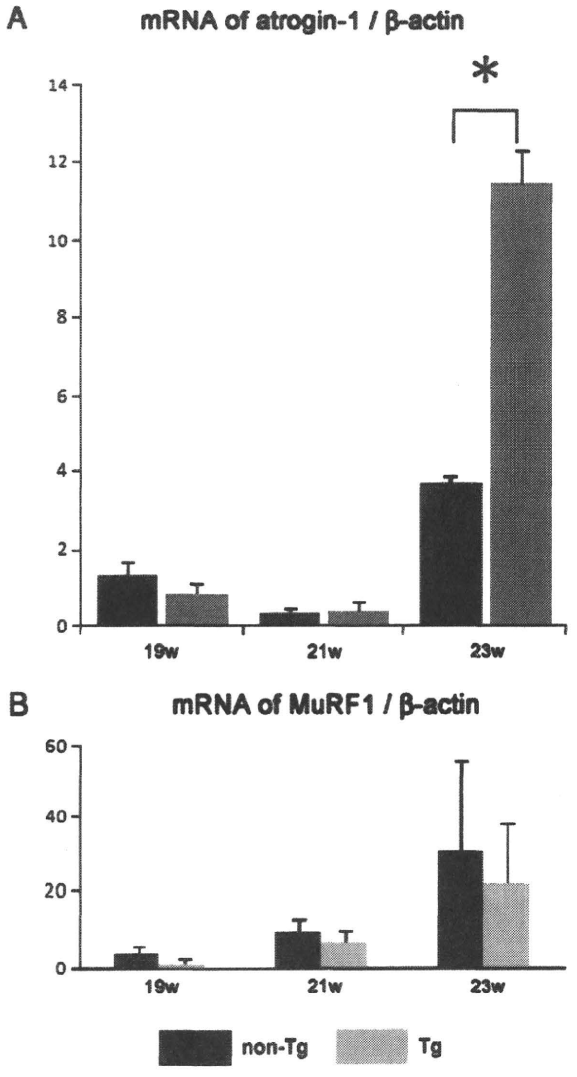

Fig. 6. Up-regulation of atrogin-1/MAFbx in the end stage of mutant SOD1 Tg mice. mRNA levels of ubiquitin ligases, atrogin-1 (A) and MuRF1 (B) ($n=5$) in Gc muscles were quantified by real time PCR. Mann–Whitney test, $^{*}p<0.05$.

cord. NO reacts rapidly with superoxide leading to the formation of peroxynitrite. nNOS, eNOS and 3-nitrotyrosine, which is a relative specific marker for peroxynitrite-mediated nitration, are selectively increased in the spinal motoneurons of sporadic and familial ALS [33]. Another study also suggested that 3-nitrotyrosine immunoreactivity is enhanced in the spinal motoneurons of sporadic and familial ALS [34].

On the other hand, there are few reports about nNOS in the skeletal muscles of ALS patients. Soraru et al. reported a reduced activity of respiratory chain complexes with mitochondrial encoded subunits and a lower nNOS amount in human ALS muscles [35]. In our study, nNOS dislocation had no relation to the extent of muscle atrophy or disease duration in this small sample size due to the variation of the disease course in human ALS. In the mutant SOD1 Tg mice model, we found increasing nNOS dislocation in the angulated muscle fibers during the disease course. In humans with ALS, we also found nNOS dislocation in the round abnormal fibers suggesting differences in the pathology between sporadic and familial ALS. In the mutant SOD1 Tg mice model, we found increasing nNOS dislocation during the disease course. We also found decreasing amounts of nNOS in the P fraction in the subcellular fractionation, suggesting the fragile connection of nNOS to the sarcolemma, although nNOS seemed to be located at the sarcolemma in the immunohistochemistry. The relatively small numbers of fibers represented by the cytosolic staining of nNOS may contribute to the comparable amount of nNOS bands in the S1 fraction of the Tg mice muscles and those of non-Tg littermates. As the mutant SOD1 Tg mice revealed the same amount of nNOS expression from the early phase of the disease, nNOS dislocation may be an upstream disease-modifying event of the muscle atrophy in the ALS pathology.

Previously, another group reported the beneficial effects of nNOS inhibition in models of motor neuron disease. Ikeda et al. reported that a nNOS inhibitor, 7-nitroindazole (7NI), potentiated grip strength and attenuated deformities in the forelimbs and reduced denervation muscle atrophy using a mouse model of motor neuron disease, Wobbler mice [36]. However, no improvement of the life span in Wobbler mice was observed. Facchinetti et al. reported that another nNOS inhibitor, ARL 17477, prolonged the survival in G93A-SOD1 Tg mice [37], but this drug is not available. Others failed to demonstrate the efficacy of nNOS in lengthening the survival of ALS Tg mice using three different nNOS inhibitors [37,38]. iNOS is abnormally expressed during the disease course of ALS, and may contribute to the unresponsiveness to nNOS inhibitors.

We previously examined the role of nNOS in denervation-induced muscle atrophy [24]. On the side denervated by cutting of the sciatic nerve, the muscle weight was significantly decreased 14 days after operation, and nNOS had already disappeared from the sarcolemma at 3 days after denervation. We observed much milder muscle atrophy in the denervated muscle of nNOS-null mice, as well as in mice injected with a nNOS inhibitor, 7-NI, or a pan-NOS inhibitor, N-(G)-nitro-L-arginine methyl ester (L-NAME) [24]. However, these drugs were revealed not to relieve the disease progression of ALS through intravenous and intranasal approaches [37,38]. Another water soluble nNOS-selective inhibitor, N5-(1-Imino-3-butenyl)-L-ornithine (L-VNIO), was proved to be active in an *in vivo* model of blood pressure [39–43]. L-VNIO may be beneficial in skeletal muscle and spinal cords in motor neuron diseases.

In conclusion, we demonstrated that nNOS dislocated from the sarcolemma to the cytoplasm may be the upstream disease-modifying event of muscle atrophy in human ALS and Tg mice. A common nNOS dislocation/atrogin-1 pathway among tail suspension, denervation and ALS induced muscle atrophy is suggested. nNOS modulation therapy may be beneficial in several types of muscle atrophy, but modulation of the drug delivery system and potentiation of the drug will be necessary.

Acknowledgements

This work was supported by Research grants from Nervous and Mental disorders (20B-13), Research on Measures for Intractable Diseases, Research on Psychiatric and Neurological Diseases and Mental Health from the Japanese Ministry of Health Labor and Welfare, Grants-in-Aids for Scientific Research (C: 19590977, 21591070) and Grants-in-Aids for Young Scientist (19890016) from the Japanese Ministry of Education, Culture, Sports, Science and Technology.

We thank Ms. N. Shimakura, K. Aihara, R. Ando, T. Nakatani, and M. Toyosawa for technical supports. We also thank Mr. Brent Bell for reading the manuscript.

References

[1] Mitchell JD, Borasio GD. Amyotrophic lateral sclerosis. Lancet 2007;369:2031–41.
[2] Miller TM, Smith RA, Cleveland DW. Amyotrophic lateral sclerosis and gene therapy. Nat Clin Pract Neurol 2006;2:462–3.
[3] Pasinelli P, Brown RH. Molecular biology of amyotrophic lateral sclerosis: insights from genetics. Nat Rev Neurosci 2006;7:710–23.

[4] Rosen DR, Siddique T, Patterson D, Figlewicz DA, Sapp P, Hentati A, et al. Mutations in Cu/Zn superoxide dismutase gene are associated with familial amyotrophic lateral sclerosis. Nature 1993;362:59–62.
[5] Aoki M, Abe K, Houi K, Ogasawara M, Matsubara Y, Kobayashi T, et al. Variance of age at onset in a Japanese family with amyotrophic lateral sclerosis associated with a novel Cu/Zn superoxide dismutase mutation. Ann Neurol 1995;37:676–9.
[6] Aoki M, Ogasawara M, Matsubara Y, Narisawa K, Nakamura S, Itoyama Y, et al. Mild ALS in Japan associated with novel SOD mutation. Nat Genet 1993;5:323–4.
[7] Nagai M, Aoki M, Miyoshi I, Kato M, Pasinelli P, Kasai N, et al. Rats expressing human cytosolic copper–zinc superoxide dismutase transgenes with amyotrophic lateral sclerosis: associated mutations develop motor neuron disease. J Neurosci 2001;21:9246–54.
[8] Sasaki S, Nagai M, Aoki M, Komori T, Itoyama Y, Iwata M. Motor neuron disease in transgenic mice with an H46R mutant SOD1 gene. J Neuropathol Exp Neurol 2007;66:517–24.
[9] Mizuno H, Warita H, Aoki M, Itoyama Y. Accumulation of chondroitin sulfate proteoglycans in the microenvironment of spinal motor neurons in amyotrophic lateral sclerosis transgenic rats. J Neurosci Res 2008;86:2512–23.
[10] Ishigaki A, Aoki M, Nagai M, Warita H, Kato S, Kato M, et al. Intrathecal delivery of hepatocyte growth factor from amyotrophic lateral sclerosis onset suppresses disease progression in rat amyotrophic lateral sclerosis model. J Neuropathol Exp Neurol 2007;66:1037–44.
[11] Tidball JG. Mechanical signal transduction in skeletal muscle growth and adaptation. J Appl Physiol 2005;98:1900–8.
[12] Ikemoto M, Nikawa T, Takeda S, Watanabe C, Kitano T, Baldwin KM, et al. Space shuttle flight (STS-90) enhances degradation of rat myosin heavy chain in association with activation of ubiquitin–proteasome pathway. FASEB J 2001;15: 1279–81.
[13] Bodine SC, Latres E, Baumhueter S, Lai VK, Nunez L, Clarke BA, et al. Identification of ubiquitin ligases required for skeletal muscle atrophy. Science 2001;294: 1704–8.
[14] Gomes MD, Lecker SH, Jagoe RT, Navon A, Goldberg AL. Atrogin-1, a muscle-specific F-box protein highly expressed during muscle atrophy. Proc Natl Acad Sci U S A 2001;98:14440–5.
[15] Bodine SC, Stitt TN, Gonzalez M, Kline WO, Stover GL, Bauerlein R, et al. Akt/mTOR pathway is a crucial regulator of skeletal muscle hypertrophy and can prevent muscle atrophy in vivo. Nat Cell Biol 2001;3:1014–9.
[16] Song YH, Li Y, Du J, Mitch WE, Rosenthal N, Delafontaine P. Muscle-specific expression of IGF-1 blocks angiotensin II-induced skeletal muscle wasting. J Clin Invest 2005;115:451–8.
[17] Rommel C, Bodine SC, Clarke BA, Rossman R, Nunez L, Stitt TN, et al. Mediation of IGF-1-induced skeletal myotube hypertrophy by PI(3)K/Akt/mTOR and PI(3)K/Akt/GSK3 pathways. Nat Cell Biol 2001;3:1009–13.
[18] Latres E, Amini AR, Amini AA, Griffiths J, Martin FJ, Wei Y, et al. Insulin-like growth factor-1 (IGF-1) inversely regulates atrophy-induced genes via the phosphatidylinositol 3-kinase/Akt/mammalian target of rapamycin (PI3K/Akt/mTOR) pathway. J Biol Chem 2005;280:2737–44.
[19] Cai D, Frantz JD, Tawa Jr NE, Melendez PA, Oh BC, Lidov HG, et al. IKKbeta/NF-kappaB activation causes severe muscle wasting in mice. Cell 2004;119:285–98.
[20] Sandri M, Sandri C, Gilbert A, Skurk C, Calabria E, Picard A, et al. Foxo transcription factors induce the atrophy-related ubiquitin ligase atrogin-1 and cause skeletal muscle atrophy. Cell 2004;117:399–412.
[21] Li YP, Schwartz RJ, Waddell ID, Holloway BR, Reid MB. Skeletal muscle myocytes undergo protein loss and reactive oxygen-mediated NF-kappaB activation in response to tumor necrosis factor alpha. FASEB J 1998;12:871–80.
[22] Acharyya S, Butchbach ME, Sahenk Z, Wang H, Saji M, Carathers M, et al. Dystrophin glycoprotein complex dysfunction: a regulatory link between muscular dystrophy and cancer cachexia. Cancer Cell 2005;8:421–32.
[23] Acharyya S, Ladner KJ, Nelsen LL, Damrauer J, Reiser PJ, Swoap S, et al. Cancer cachexia is regulated by selective targeting of skeletal muscle gene products. J Clin Invest 2004;114:370–8.
[24] Suzuki N, Motohashi N, Uezumi A, Fukada S, Yoshimura T, Itoyama Y, et al. NO production results in suspension-induced muscle atrophy through dislocation of neuronal NOS. J Clin Invest 2007;117:2468–76.
[25] Koyama S, Arawaka S, Chang-Hong R, Wada M, Kawanami T, Kurita K, et al. Alteration of familial ALS-linked mutant SOD1 solubility with disease progression: its modulation by the proteasome and Hsp70. Biochem Biophys Res Commun 2006;343:719–30.
[26] Kato M, Aoki M, Ohta M, Nagai M, Ishizaki F, Nakamura S, et al. Marked reduction of the Cu/Zn superoxide dismutase polypeptide in a case of familial amyotrophic lateral sclerosis with the homozygous mutation. Neurosci Lett 2001;312:165–8.
[27] Aoki M, Kato S, Nagai M, Itoyama Y. Development of a rat model of amyotrophic lateral sclerosis expressing a human SOD1 transgene. Neuropathology 2005;25: 365–70.
[28] Sasaki S, Aoki M, Nagai M, Kobayashi M, Itoyama Y. Mitochondrial alterations in transgenic mice with an H46R mutant Cu/Zn superoxide dismutase gene. J Neuropathol Exp Neurol 2009;68:365–73.
[29] Brenman JE, Chao DS, Xia H, Aldape K, Bredt DS. Nitric oxide synthase complexed with dystrophin and absent from skeletal muscle sarcolemma in Duchenne muscular dystrophy. Cell 1995;82:743–52.
[30] Leger B, Vergani L, Soraru G, Hespel P, Derave W, Gobelet C, et al. Human skeletal muscle atrophy in amyotrophic lateral sclerosis reveals a reduction in Akt and an increase in atrogin-1. FASEB J 2006;20:583–5.
[31] Kato N, Sato S, Yokoyama H, Kayama T, Yoshimura T. Sequential changes of nitric oxide levels in the temporal lobes of kainic acid-treated mice following application of nitric oxide synthase inhibitors and phenobarbital. Epilepsy Res 2005;65:81–91.
[32] Kim SF, Huri DA, Snyder SH. Inducible nitric oxide synthase binds, S-nitrosylates, and activates cyclooxygenase-2. Science 2005;310:1966–70.
[33] Beal MF, Ferrante RJ, Browne SE, Matthews RT, Kowall NW, Brown Jr RH. Increased 3-nitrotyrosine in both sporadic and familial amyotrophic lateral sclerosis. Ann Neurol 1997;42:644–54.
[34] Cassina P, Peluffo H, Pehar M, Martinez-Palma L, Ressia A, Beckman JS, et al. Peroxynitrite triggers a phenotypic transformation in spinal cord astrocytes that induces motor neuron apoptosis. J Neurosci Res 2002;67:21–9.
[35] Soraru G, Vergani L, Fedrizzi L, D'Ascenzo C, Polo A, Bernazzi B, et al. Activities of mitochondrial complexes correlate with nNOS amount in muscle from ALS patients. Neuropathol Appl Neurobiol 2007;33:204–11.
[36] Ikeda K, Iwasaki Y, Kinoshita M. Neuronal nitric oxide synthase inhibitor, 7-nitroindazole, delays motor dysfunction and spinal motoneuron degeneration in the Wobbler mouse. J Neurol Sci 1998;160:9–15.
[37] Facchinetti F, Sasaki M, Cutting FB, Zhai P, MacDonald JE, Reif D, et al. Lack of involvement of neuronal nitric oxide synthase in the pathogenesis of a transgenic mouse model of familial amyotrophic lateral sclerosis. Neuroscience 1999;90: 1483–92.
[38] Martinez JA, Francis GJ, Liu WQ, Pradzinsky N, Fine J, Wilson M, et al. Intranasal delivery of insulin and a nitric oxide synthase inhibitor in an experimental model of amyotrophic lateral sclerosis. Neuroscience 2008;157:908–25.
[39] Talman WT, Dragon DN. Transmission of arterial baroreflex signals depends on neuronal nitric oxide synthase. Hypertension 2004;43:820–4.
[40] Yamaleyeva LM, Gallagher PE, Vinsant S, Chappell MC. Discoordinate regulation of renal nitric oxide synthase isoforms in ovariectomized mRen2.Lewis rats. Am J Physiol Regul Integr Comp Physiol 2007;292:R819–26.
[41] Kakoki M, Zou AP, Mattson DL. The influence of nitric oxide synthase 1 on blood flow and interstitial nitric oxide in the kidney. Am J Physiol Regul Integr Comp Physiol 2001;281:R91–7.
[42] Babu BR, Griffith OW. N5-(1-Imino-3-butenyl)-L-ornithine. A neuronal isoform selective mechanism-based inactivator of nitric oxide synthase. J Biol Chem 1998;273:8882–9.
[43] Burkard N, Rokita AG, Kaufmann SG, Hallhuber M, Wu R, Hu K, et al. Conditional neuronal nitric oxide synthase overexpression impairs myocardial contractility. Circ Res 2007;100:e32–44.

OPEN ACCESS Freely available online

PLoS one

An Inducer of VGF Protects Cells against ER Stress-Induced Cell Death and Prolongs Survival in the Mutant SOD1 Animal Models of Familial ALS

Masamitsu Shimazawa[1], Hirotaka Tanaka[1], Yasushi Ito[1], Nobutaka Morimoto[1], Kazuhiro Tsuruma[1], Michinori Kadokura[2], Shigeki Tamura[2], Teruyoshi Inoue[2], Mitsunori Yamada[3], Hitoshi Takahashi[4], Hitoshi Warita[5], Masashi Aoki[5], Hideaki Hara[1]*

1 Molecular Pharmacology, Department of Biofunctional Evaluation, Gifu Pharmaceutical University, Gifu, Japan, 2 Biomedical Research Laboratories, Asubio Pharma Co., Ltd., Osaka, Japan, 3 Department of Clinical Research, National Hospital Organization, Saigata National Hospital, Niigata, Japan, 4 Department of Pathology, Brain Research Institute, Niigata University, Niigata, Japan, 5 Department of Neurology, Tohoku University School of Medicine, Sendai, Japan

Abstract

Amyotrophic lateral sclerosis (ALS) is the most frequent adult-onset motor neuron disease, and recent evidence has suggested that endoplasmic reticulum (ER) stress signaling is involved in the pathogenesis of ALS. Here we identified a small molecule, SUN N8075, which has a marked protective effect on ER stress-induced cell death, in an *in vitro* cell-based screening, and its protective mechanism was mediated by an induction of VGF nerve growth factor inducible (VGF): VGF knockdown with siRNA completely abolished the protective effect of SUN N8075 against ER-induced cell death, and overexpression of VGF inhibited ER-stress-induced cell death. VGF level was lower in the spinal cords of sporadic ALS patients than in the control patients. Furthermore, SUN N8075 slowed disease progression and prolonged survival in mutant SOD1 transgenic mouse and rat models of ALS, preventing the decrease of VGF expression in the spinal cords of ALS mice. These data suggest that VGF plays a critical role in motor neuron survival and may be a potential new therapeutic target for ALS, and SUN N8075 may become a potential therapeutic candidate for treatment of ALS.

Citation: Shimazawa M, Tanaka H, Ito Y, Morimoto N, Tsuruma K, et al. (2010) An Inducer of VGF Protects Cells against ER Stress-Induced Cell Death and Prolongs Survival in the Mutant SOD1 Animal Models of Familial ALS. PLoS ONE 5(12): e15307. doi:10.1371/journal.pone.0015307

Editor: Rafael Linden, Universidade Federal do Rio de Janeiro, Brazil

Received September 13, 2010; **Accepted** November 5, 2010; **Published** December 9, 2010

Funding: This work was supported in part by the Japanese Ministry of Health Labor and Welfare and Takeda Science Foundation. The funders had no role in study design, data collection and analysis, decision to publish, or preparation of the manuscript. No additional external funding received for this study.

Competing Interests: The authors have declared that no competing interests exist.

* E-mail: hidehara@gifu-pu.ac.jp

Introduction

In chronic neurodegenerative disorders such as Alzheimer's disease, Parkinson's disease, Huntington's disease (HD), and amyotrophic lateral sclerosis (ALS), abnormally unfolded proteins are known to aggregate and accumulate in neurons, and these proteins are thought to be closely related to the initiation and development of these neurodegenerative diseases [1,2,3]. Recent studies suggest that endoplasmic reticulum (ER) stress plays a role in the pathogenesis of familial and sporadic ALS [4,5,6]. A variety of conditions such as environmental and genetic causes that cause unfolded or misfolded proteins in the ER can activate the ER stress response although the cell normally survives the insult. However, excessive or prolonged ER stress can induce cell death, usually in the form of apoptosis. In familial ALS model mice carrying the mutant SOD1 gene, mutant superoxide dismutase-1 forms aggregates in the ER have been reported to induce the expression of 78 kDa glucose-regulated protein (GRP78/BiP), an ER resident molecular chaperone, and to activate caspase-12, leading to neuronal cell death [7,8]. Furthermore, Ilieva et al. [6] have reported increased ER chaperones such as protein-disulfide isomerase (PDI) and phosphorylation of eukaryotic initiation factor 2α (eIF2α) in spinal cords from patients with sporadic ALS. Thus, although the etiologies such as the responsible genes or environmental factors are different for familial and sporadic ALS, they may have a common mechanism for neuronal cell death through ER stress as downstream signaling pathways. Despite many clinical trials for treatment of ALS, there has been little success in the search for neuroprotective agents. Therefore, we screened for protecting cells from ER stress, and identified a small molecule, SUN N8075 (Fig. 1A). SUN N8075 has been reported to have a potent antioxidant property [9], and is currently in a phase I clinical trial for stroke. In the present study, we demonstrated that SUN N8075 induces VGF nerve growth factor inducible (VGF) as a mechanism for protecting ER stress-induced cell death in an antioxidant-independent manner. VGF is a neuronal polypeptide first identified as a cDNA clone from plate V of the nerve growth factor (NGF)-induced rat pheochromocytoma (PC12) cell cDNA library [10]. VGF is widely expressed in neurons in the brain and involved in maintaining organism energy balance, as well as in mediating hippocampal synaptic activity [11,12]. Interestingly, a recent study reported that VGF content was decreased in the cerebrospinal fluid (CSF) of ALS patients and in the serum, CSF and spinal cord motor neurons of G93A mice [13]. These findings strongly suggest that a VGF inducer, SUN N8075, may become a potential therapeutic candidate for ALS. In the present study, we demonstrated that (i) VGF is involved in the protective effects of SUN N8075 on ER stress-induced cell death

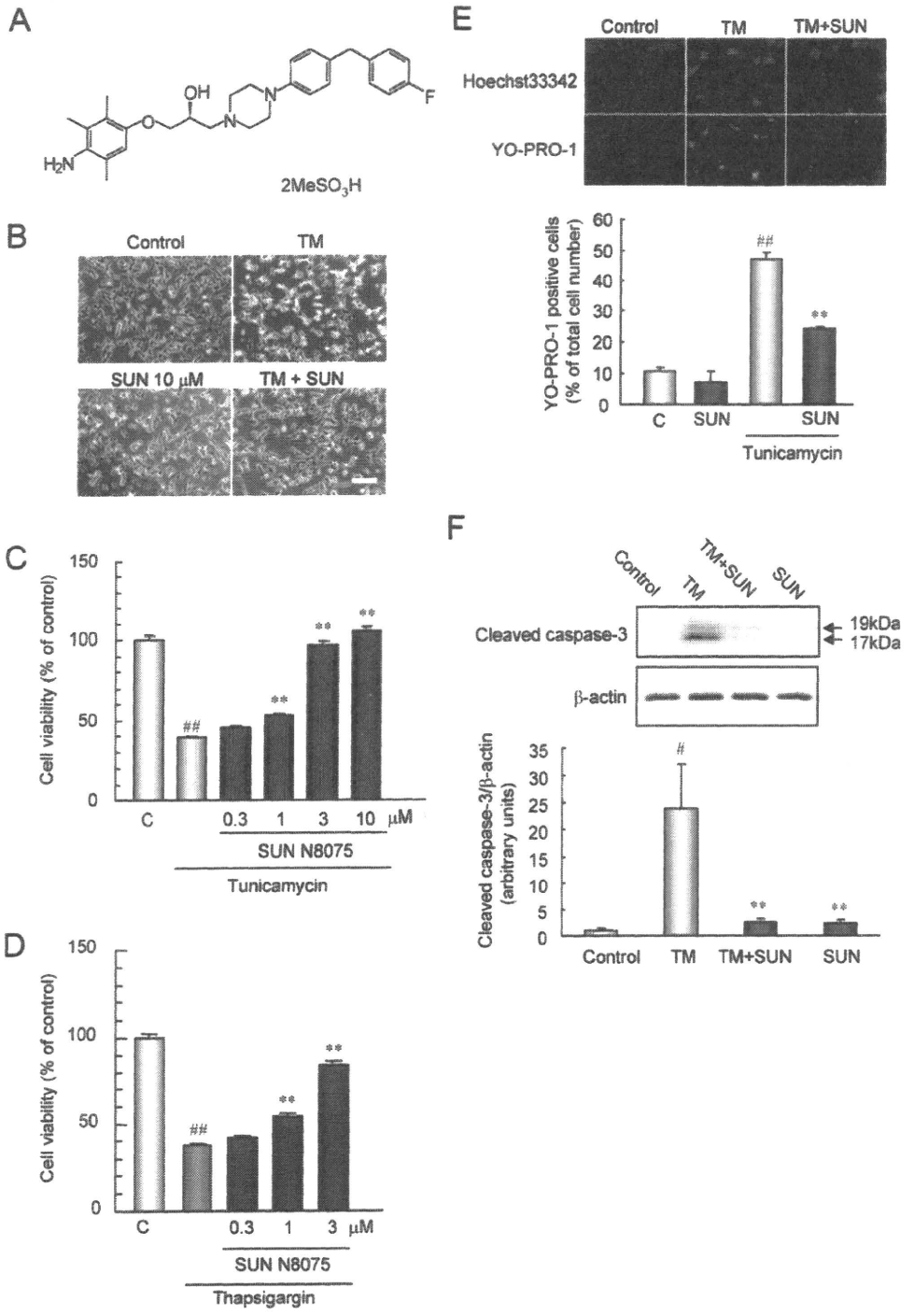

Figure 1. SUN N8075 protects against ER stress-induced cell death and attenuates cleaved caspase-3 production. (A) Chemical structure of SUN N8075, (B) Representative phase-contrast microscopy showing the effect of SUN N8075 on morphological changes in SH-SY5Y cells after tunicamycin at 2 μg/ml. Bar = 50 μm. (C, D) Cell damage was induced by tunicamycin (2 μg/ml) or thapsigargin (2 μM), and cell viability was measured with the tetrazolium salt (WST-8) reduction test. SUN N7085 or vehicle was applied 1 h before the tunicamycin or thapsigargin treatment. Each column represents the mean ± S.E.M. ($n = 8$). ##$p<0.01$ versus control. **$p<0.01$ versus tunicamycin or thapsigargin alone. (E) Representative fluorescence microscopy showing nuclear stainings for Hoechst 33342 (blue) and YO-PRO-1 (green) at 24 h after the addition of 2 μg/ml of tunicamycin with or without SUN N8075. Each column represents the mean ± S.E.M. (n = 6). ** and ##$p<0.01$ versus relevant control group. (F) Tunicamycin increased cleaved caspase-3, and treatment with SUN N8075 inhibited the increase of cleaved caspase-3 after tunicamycin. Each column represents the mean ± S.E.M. ($n = 6$). #$p<0.05$ versus control. **$p<0.01$ versus tunicamycin alone.
doi:10.1371/journal.pone.0015307.g001

and (ii) SUN N8075 protects against disease progression and prolongs survival in familial ALS models involving ER stress.

Materials and Methods

Chemicals

(2S)-1-(4-Amino-2,3,5-trimethylphenoxy)-3-{4-[4-(4-fluorobenzyl) phenyl]-1-piperazinyl}-2-propanol dimethanesulfonate (SUN N8075) was synthesized at Asubio Pharma Co. Ltd. (Osaka, Japan).

Cell cultures

Cultures of human neuroblastoma (SH-SY5Y) cells were maintained in Dulbecco's modified Eagles's medium (D-MEM, St. Louis, MO) containing 10% FBS (Valeant, Costa Mesa, CA), 100 U/ml penicillin (Meiji Seika Kaisha Ltd., Tokyo, Japan), and 100 μg/ml streptomycin (Meiji Seika Kaisha Ltd.) in a humidified atmosphere of 95% air and 5% CO_2 at 37°C. The cells were passaged by trypsinization every 5 to 7 days, as described in a previous report [14].

ER stress-induced cell death

To examine the effects of the SUN N8075 on tunicamycin-induced cell death, cells were seeded at a density of 1×10^4 cells per well into 96-well plates, and then incubated in a humidified atmosphere of 95% air and 5% CO_2 at 37°C for 2 days. Tunicamycin (Wako, Osaka, Japan) or thapsigargin was added to the cells at a final concentration of 2 μg/ml and 2 μM, respectively. SUN N8075 was added 1 h before the tunicamycin treatment, at which time the cell-culture medium was replaced with D-MEM containing 1% FBS. Assessment of cell viability was performed using two methods, each at 24 h after the addition of tunicamycin. The first method was a single-cell digital imaging-based method employing fluorescent staining of nuclei. Cell death was assessed on the basis of combination staining with fluorescent dyes [namely, Hoechst 33342 and YO-PRO-1 (Molecular Probes, Eugene, OR)], observations being made using an OLYMPUS IX70 inverted epifluorescence microscope (OLYMPUS, Tokyo, Japan). Hoechst 33342 freely enters living cells and therefore stains the nuclei of viable cells, as well as those that have suffered apoptosis or necrosis. Apoptotic cells can be distinguished from viable and necrotic cells on the basis of nuclear condensation and fragmentation. YO-PRO-1 is a membrane-impermeant dye that is generally excluded from viable cells, whereas early-stage apoptotic and necrotic cells are YO-PRO-1-positive. At the end of the culture period, Hoechst 33342 and YO-PRO-1 dyes were added to the culture medium (at 8 and 0.1 μM, respectively) for 30 min. Images were collected using a digital camera (COOLPIX 4500, Nikon, Tokyo, Japan). In a blind manner, a total of at least 400 cells per condition were counted using image-processing software (Image-J ver. 1.33f; National Institutes of Health, USA). As the second method for measuring cell viability, cell metabolic activity was quantitatively assessed. Cell viability was assessed following immersion in 10% WST-8 solution [2-(2-methoxy-4-nitrophenyl)-3-(4-nitrophenyl)-5-(2,4-disulfophenyl)-2H-tetrazolium, monosodium salt] with an electron carrier, 1-Methoxy PMS (1-Methoxy-5-methylphenazinium, methylsulfate) (Cell Counting Kit-8, Dojin Kagaku, Kumamoto, Japan) for 3 h at 37°C, and absorbance was recorded at 450 nm [15]. WST-8 is bioreduced by cellular dehydrogenases to an orange formazan product that is soluble in cell culture medium. The amount of formazan produced is directly proportional to the number of living cells. This absorbance is expressed as a percentage of that in control cells, after subtraction of background absorbance.

Immunoblotting

SH-SY5Y cells or mouse spinal cords were lysed using a cell-lysis buffer [RIPA buffer (R0278; Sigma) with protease (P8340; Sigma) and phosphatase inhibitor cocktails (P2850 and P5726; Sigma), and 1 mM EDTA]. Lysates were solubilized in SDS-sample buffer, separated on 10% SDS-polyacrylamide gels, and transferred to PVDF membrane (Immobilon-P; Millipore, Bedford, MA). Transfers were blocked for 1 h at room temperature with 5% Blocking One-P (Nakarai Tesque, Inc., Kyoto, Japan) in 10 mM Tris-buffered saline with 0.05% Tween 20 (TBS-T), then incubated overnight at 4°C with the primary antibody. The transfers were then rinsed with TBS-T and incubated for 1 h at room temperature in horseradish peroxidase goat anti-rabbit or goat anti-mouse (Pierce, Rockford, IL) diluted 1:2000. The immunoblots were developed using chemiluminescence (Super Signal® West Femto Maximum Sensitivity Substrate; Pierce), and visualized with the aid of a digital imaging system (FAS-1000; TOYOBO CO., LTD, Osaka, Japan). The primary antibodies used were as follows: mouse anti-cleaved caspase-3 (#9661, Cell Signaling, Beverly, MA), rabbit anti-VGF (SantaCruz, Santa Cruz, CA) and rabbit anti-β-actin (clone AC-74, Sigma-Aldrich, Saint Luis, MO).

Real-time PCR

To examine the effect of SUN N8075 on VGF mRNA expression, SH-SY5Y cells were seeded in 96-well plates at a density of 1.0×10^4 cells per well. After the cells had been incubating for 48 h, they were exposed to tunicamycin at 2 μg/ml with or without SUN N8075 at 3 μM in 1% FBS DMEM for 2, 6, or 12 h. Quantitative real-time PCR was performed using a Thermal Cecler Real Time System (TP-800, Takara) with a TaqMan® Gene Expression Cells-to-CT™ Kit (Applied Biosystems) according to the manufacturer's protocol. mRNA expression was measured by real-time PCR using TaqMan probe (TaqMan Gene Expression Assay): VGF (Assay ID Details: Hs00705044_s1). The thermal cycler conditions were as follows: 2 min at 50°C and then 10 min at 95°C, followed by two-step PCR for 50 cycles consisting of 95°C for 15 sec followed by 60°C for 1 min. For each PCR, we obtained the slope value, R2 value, and linear range of a standard curve of serial dilutions. The results are expressed relative to the GAPDH (#4333764T, Applied Biosystems) internal control.

VGF knockdown and overexpression

For VGF knockdown, the following siRNA sequences specific to human VGF were used: 5′-AUUCACUCGGGUCAGCGUGUGCGUG-3′ (sense), 5′-CACGCACACGCUGACCCGAGUGAAU-3′ (antisense). Stealth™ RNAi Negative Control Medium GC Duplex #2 was used as a control. All siRNAs were obtained from Invitrogen (Carlsbad, CA, USA). The SH-SY5Y cells were transfected with 50 pg of siRNA using Lipofectamine™ RNAi MAX Reagent (Invitrogen) according to the manufacturer's protocol.

For overexpression of VGF, pCMV6-ENTRY containing myc-tagged VGF and same empty vector (control) were obtained from ORIGENE (Rockville, MD, USA). SH-SY5Y cells were transiently transfected with each plasmid using Lipofectamine™2000 (Invitrogen) according to the manufacturer's protocol. The transfected cells were subjected to immunoblot analysis and cell death assay. The cells transiently transfected with plasmids or siRNAs were incubated for 24 h at 37°C in a humidified atmosphere of 95% air and 5% CO_2.

Animals

We used two types of transgenic animals overexpressing mutated human SOD1 genes: transgenic mice overexpressing mutated (glycine to alanine in position 93) human SOD1 (G93A) [16] and transgenic rats overexpressing mutated (histidine to arginine in position 46) human SOD1 (H46R) [17]. The transgenic G93A [B6SJL-Tg (SOD1-G93A) 1Gur/J] mice were purchased from the Jackson Laboratory (Bar Harbor, ME, USA). The hemizygous SOD1G93A mice were maintained by mating transgenic males with wild-type (WT) females. Mouse genotypes were determined by polymerase chain reaction analysis as previously reports [16,18]. The transgenic male H46R rats were used a colony generated in Tohoku University Graduate School of Medicine as a previous report [17]. All experiments were approved and monitored by the Institutional Animal Care and Use Committee of Gifu Pharmaceutical University (Permit Number: 08-085, 2008-366).

Drugs

SUN N8075 was dissolved in 6% captisol solution, and subcutaneously administered at doses of 30 mg/kg and 10 mg/kg, respectively, once daily from 10-weeks-old (for SOD1G93A mice) or 15-weeks-old (for SOD1H46R rat) to lifetime. In control group, vehicle (6% captisol solution) was subcutaneously administered at 10 ml/kg.

Rotarod test

A rotarod test was performed with a rotation at 5 rpm once every 7 days, as previously described by Chiba et al. [19]. Mice, which did not learn to remain on the rod for 600 s, were excluded from motor performance analysis. The disease onset was defined as the day when a mouse first dropped off the rotarod within 600 s.

Motor score

Symptomatic disease onset and post-symptomatic disease progression were assessed using a 5-point motor score system as described in previous reports [20]. This assay was performed once per day until the disease end-point. Rats were allowed to move freely in open field and were scored blindly by a single observer (H.T.). The scoring system was used following these scales: 5, normal movement; 4, limping or dragging of any limb, however still able to stand on hindlimbs; 3, dragging of lower body and inability to stand on hindlimbs; 2, Unable to drag the lower body, however righting reflexes present from both side; 1, a righting reflex from only one side; 0, absent righting reflexes from both sides within 30 second. This point was defined as the end-point and lifespan was determined by the age of the rats at end-point. Symptomatic onset was identified when the score showed 4.

Survivals

Mortality was scored at the day when the mouse was unable to right itself within 30 s after being placed on its back.

Microarray analysis

Total RNA was extracted from SH-SY5Y using the RNeasy Mini kit (Qiagen, Westburg, Leusden, NL, USA) including a DNase digestion step, according to the manufacturer's instructions. Total RNA was amplified and labeled with Cyanine 3 for the test sample using Agilent's Low RNA Input Linear Amplification Kit (Agilent Technologies, Palo Alto, CA) following the detailed protocol described in the kit manual (version 5.7). Briefly, 500 ng of total RNA was reversed transcribed to double-strand cDNA using a poly dT-T7 promoter primer. Primer, template RNA and quality-control transcripts of known concentration and quality were first denatured at 65°C for 10 min and incubated for 2 hours at 40°C with 5× first strand Buffer, 0.1 M DTT, 10 mM dNTP, MMLV RT, and RNase-out. The MMLV-RT enzyme was inactivated at 70°C for 15 min. cDNA products were then used as templates for in vitro transcription to generate fluorescent cRNA. cDNA products were mixed with a transcription master mix in the presence of T7 RNA polymerase and Cy3 labeled-CTP and incubated at 40°C for 2 h. Labeled cRNAs were purified using Qiagen's RNeasy mini spin columns and eluted in 30 µL of nuclease-free water. After amplification and labeling, cRNA quantity and cyanine incorporation were determined using a NanoDrop ND. Microarray expression experiments were performed on 4×44 K Agilent Human and Mouse expression arrays (Agilent technologies) by hybridizing SH-SY5Y cells according to the manufacturer's instructions. Images of the arrays were acquired using a microarray scanner G2565BA (Agilent technologies) and image analysis was performed using Feature Extraction software version 9.5 (Agilent Technologies).

Gene expression data analyses (statistical analysis and hierarchical clustering analysis)

Raw data was imported into GeneSpring GX 7.3.1 (Agilent Technologies) and normalized by setting all measurements <0.01 to 0.01, normalizing each chip to the 75th percentile of all measurements taken for that chip, and normalizing each gene to the median measurement for that gene across all chips. To focus on genes with reliable measurements, the normalized data were filtered for data that had present call in ≥33% of all samples (based on flag information of Agilent Feature Extraction Software v.9.5.3) and the genes chosen by parametric test (don't assume variances equal) with a Bejamini and Hochberg false discovery rate (FDR) <0.01 and twofold restriction filters were utilized. Hierarchical clustering was performed on the log transformed normalized data of all the samples. Pearson's correlation was used for the similarity metric and the calculation result was visualized using "Gene Tree" algorism. A red/blue color scheme was used in the heat maps of the gene expressions.

Tissue Preparation

SOD1G93A and WT mice at 14 weeks of age (decreasing motor function) were anesthetized with sodium pentobarbital (80 mg/kg, i.p.) (Nembutal, Dainippon, Osaka, Japan) and perfused with 2% (w/v) paraformaldehyde solution in 0.01 M phosphate-buffered saline (PBS) at pH 7.4. Spinal cord tissues were removed after a 15-min perfusion at 4°C and immersed in the same fixative solution for 24 h. Each spinal cord included L1, L2, and L3 levels, were soaked in 25% (w/v) sucrose at 4°C for 1 day, and then frozen in embedding compound (Tissue-Tek, Sakura Finetechnical Co. Ltd., Tokyo, Japan). Embedded tissues were immediately frozen with liquid nitrogen and stored at −80°C. Serial transverse sections were cut on a cryostat to a thickness of 20 µm at 2-mm intervals (3 sections total for each segment) and used for cresyl violet staining or immunohistochemistry.

Human spinal cord

Spinal cord segments were taken at autopsy from ten patients with features typical of sporadic ALS. Spinal cord tissue from 6 individuals without history/evidence of neurological or psychiatric disease was taken for the control samples (Table S1). Three paraffin-embedded coronal sections cut at 4-µm thickness through the spinal cord [cervical spinal cord (C7), thoracic spinal cord (T8),

and lumbar spinal cord (L4)] were prepared in the standard manner. The research protocol was approved by the institutional ethics committee of Niigata University, and informed consent was obtained from all participants.

Immunohistochemistry

The sections were stained with the following antibodies: (i) mouse anti-VGF monoclonal antibody (1:50; Santa Cruz Biotechnology, Santa Cruz, CA, USA); (ii) goat anti-NeuN polyclonal antibody (1:5000; Millipore, Bedford, MA, USA); (iii) mouse anti-GFAP monoclonal antibody (1:1000; Millipore); and (iv) mouse anti-CD11b monoclonal antibody (1:1000; BMA Biomedicals, Augst, Switzerland) within Can Get Signal immunostain solution A (Toyobo CO., LTD., Osaka, Japan). Sections were treated with 0.3% H_2O_2 in methanol for 30 min at room temperature and blocking with mouse-on-mouse blocking reagent for 1 h at room temperature. Anti-VGF antibody was applied to the sections for overnight at 4°C. After washing the sections with 0.01 M PBS, sections were incubated with biotinylated anti-mouse IgG for 2 h followed by washing, and were incubated with the avidin-biotin-peroxidase complex for 30 min at room temperature. The sections were finally visualized using diamino benzidine/H_2O_2 substrate for peroxidase (Vector Laboratories, Inc., Burlingame, CA).

For paraffin embedding human spinal cord sections, conventional antigen retrieval method for each antigen was performed at its optimal condition with 0.01 M sodium citrate buffer, pH 7.4. Next, coronal sections of spinal cord were washed with 0.01 M PBS, and then treated with 0.3% hydrogen peroxidase in 0.01 M PBS for 30 min at room temperature. Furthermore, the sections were preincubated with 10% normal horse serum (Vector) in 0.01 M PBS for 30 min and then incubated for 1 h at room temperature with specific goat anti-VGF polyclonal antibody (R-15; 1:50, Santa Cruz Biotechnology, CA, USA) in the following solution: 10% normal horse serum in 0.01 M PBS containing 0.3% (v/v) Triton X-100. They were washed with 0.01 M PBS and then incubated with biotinylated anti-goat IgG before being incubated with the avidin-biotin-peroxidase complex for 30 min at room temperature, and finally visualized using diamino benzidine/H_2O_2 substrate. To assess intensity of VGF immunoreactivity in the Rexed laminae IX anterior horn (AH) in the human spinal cord, sections immunostained with VGF were used for the intensity measurement: C7, T8, and L4 in the spinal cords of the control patients and patients with sporadic ALS, respectively. The volume used for the intensity measurement was 438×330×4 μm (section thickness) of each side in the spinal cord. The density measurements were carried out under objective ×40 with bright-field microscope in a masked fashion by a single observer (Y.I.). Anti-VGF antibody revealed the expression pattern of VGF in spinal cord. The density on each section was measured using MetaMorph software (Molecular Devices). Data from each section was averaged for each spinal cord, and the values obtained were used to evaluate the density of VGF immunoreactivity.

When double-immunostaining for VGF/GFAP, VGF/NeuN, or VGF/CD11b were performed, these antibodies were applied to the sections for overnight at 4°C after blocking with 0.01 M PBS containing 10% normal goat serum (Vector) or mouse-on-mouse blocking reagent (M.O.M. immunodetection kit, Vector) for 1 h. After washing the sections with 0.01 M PBS, immunoreactivity was visualized by incubating them for 2 h at room temperature with secondary antibodies conjugated with Alexa 488 rabbit anti-mouse, Alexa 546 rabbit anti-goat, Alexa 488 goat anti-rabbit, or Alexa 546 goat anti-mouse (1:1000; Invitrogen Japan K.K., Tokyo, Japan). At the end of immunostaining, Hoechst 33342 (1:1000) was added to the samples for 30 min to visualize nucleus.

Total images of the spinal cord were taken using a microscope (BX50; Olympus, Tokyo, Japan) fitted with ×20 and ×40 microscope objective lenses. The images visualized by diamino benzidine were taken using a charge-coupled device camera (MicroPublisher 5.0RTV, QIMAGING, Burnaby, BC, Canada) and immunofluorescence images were taken using a cooled charge-coupled device camera (DP30BP; Olympus) at 1360×1024 pixels via Metamorph (Universal Imaging Corp., Downingtown, PA, USA).

Data Analysis

Data are presented as means ± S.E.M. Statistical comparisons were made by Dunnet's test, Tukey test, or Student's *t*-test using a SPSS 16.0 (SPSS Inc., IL, USA). Statistical analysis of the cumulative probability of survival was performed with the Kaplan–Meier life test. Statistical analysis of the mean age of onset and survival was performed with log-rank test. A value of $P<0.05$ was considered to indicate a statistical significance.

Further Materials and Methods used in the supplemental Figures and Tables were described in the supporting information (Methods S1).

Results

SUN N8075 protects against cell death induced by ER stress

Representative photographs in cell morphology occurring 24 h after tunicamycin treatment at 2 μg/ml are shown in Fig. 1B. An increase in non-adherent cells was observed at 24 h after tunicamycin treatment compared with that in non-treated control cells. Pretreatment with SUN N8075 at 10 μM reduced the increase in non-adherent cells. SUN N8075 at 0.3 to 10 μM concentration-dependently inhibited the reduction of cell viability 24 h after tunicamycin treatment, its effect being significant at 1, 3 and 10 μM (Fig. 1C). Furthermore, SUN N8075 at 0.3 to 3 μM concentration-dependently inhibited the reduction of cell viability 24 h after thapsigargin treatment, and its effect being significant at 1 and 3 μM (Fig. 1D). Next, we evaluated cell death using fluorescence stainings of nuclei with Hoechst 33342 and YO-PRO-1 dyes (Fig. 1E). Non-treated control cells displayed normal nuclear morphology and negative staining with YO-PRO-1 dye, which stains early apoptotic and later-stage cells (Fig. 1E). Treatment with tunicamycin for 24 h led to shrinkage and condensation of nuclei, and to positive staining with YO-PRO-1 dye (Fig. 1E). Treatment with SUN N8075 at 3 μM reduced the tunicamycin-induced morphological changes in the nuclei and the number of cells stained with YO-PRO-1 (Fig. 1E). The number of cells exhibiting YO-PRO-1 fluorescence was counted, and the positive cells were expressed as the percentage of YO-PRO-1- to Hoechst 33342-positive cells (Fig. 1E). Twenty-four hours after the treatment with tunicamycin, the percentage of YO-PRO-1-positive cells was 47.1±3.5% ($n=8$), while in the control group, the percentage (supplemented with 1% FBS) was 10.7±1.3% ($n=8$). Treatment with SUN N8075 at 3 μM significantly reduced the increase in YO-PRO-1-positive cells induced by tunicamycin. Exposure to tunicamycin elevated the level of caspase-3 activity, indicative of an early stage of ER stress-induced apoptosis [21]. To determine the mechanism underlying the action of tunicamycin, we examined the effect of SUN N8075 on the increases in cleaved caspase-3 induced by treatment with tunicamycin. Tunicamycin increased cleaved caspase-3 proteins (Fig. 1F), and pretreatment with SUN N8075 at 10 μM significantly reduced the increase in

cleaved caspase-3 protein. On the other hand, treatment with SUN N8075 alone at 10 μM had little effect on the production of cleaved caspase-3 (versus the vehicle-treated controls). SUN N8075 has a potent antioxidant property [9], and therefore, the protective effects of SUN N8075 on ER stress-induced cell death may be derived from its antioxidative effect. However, antioxidants, *N*-acetyl-cysteine (NAC) at 1 mM or edaravone at 1 to 10 μM, did not show any effects on the reduction of cell viability after tunicamycin (Fig. S1A,B). Furthermore, NAC at 1 mM, edaravone at 10 μM or trolox at 100 μM also did not inhibit the reduction of cell viability after treatment with thapsigargin (Fig. S1C). These data suggest that the protective effects of SUN N8075 on ER stress-induced cell death are mediated by a mechanism other than antioxidant effect. On the other hand, SUN N8075 and antioxidants both inhibited the reduction of cell viability in mouse neuronal precursor cells (RGC-5) after serum deprivation or intrinsic oxidative stress induced by L-buthionine-(S,R)-sulfoximine (BSO) plus glutamate, suggesting that SUN N8075 protected cell damage against other stresses depending on the antioxidative effect (Fig. S2).

Gene expression analyses

ER stress activates signaling pathways, including the unfolded protein response (UPR) that counteracts the effects of the original stress. BiP acts as an ER-resident molecular chaperone that is induced by ER stress, and this protein refolds the unfolded proteins, thereby tending to maintain homeostasis in the ER [22,23]. C/EBP-homologous protein (CHO) is a member of the CCAAT/enhancer-binding protein family that is induced by ER stress and participates in ER-mediated apoptosis [24]. UPR is mediated by three types of ER transmembrane proteins: inositol-requiring protein-1 (IRE1), RNA-dependent protein kinase–like ER eukaryotic translation initiation factor 2α kinase (PERK), and activating transcription factor 6 (ATF6) [1], and expression of both BiP and CHOP mRNAs are upregulated by activation of these pathways. To determine whether SUN N8075 can affect the UPR after ER stress, BiP and CHOP mRNAs was quantitated with real-time PCR. Tunicamycin induced BiP and CHOP expression in a time-dependent manner (Fig. S3). SUN N8075 at a concentration of 3 μM did not show any effects on these increases after treatment with tunicamycin (Fig. S3). Furthermore, we examined cell viability and protein expression of ATF4, BiP and CHOP after tunicamycin with or without SUN N8075 in RGC-5 (Fig. S4)). SUN N8075 inhibited the reduction of cell viability induced by tunicamycin (Fig. S4A), but it did not affect the expression of ATF4, BiP, or CHOP protein at 24 h after tunicamycin treatment (Fig. S4B). These data suggest that SUN N8077 does not affect the UPRs themselves.

To generate gene expression profiles after treatment with SUN N8075 or tunicamycin, we performed microarray analyses on 4×44 K Agilent Human expression arrays by hybridizing RNA from SH-SY5Y. At least more than 26,000 genes out of 41,000 gene probes on the array were detected in each sample, and a representative scatter plot comparison in gene expression with DNA microarray between SUN N8075 and vehicle control treatments at 7 h is shown in Fig. 2A. Heat map representation of the hierarchical clustering of 320 genes with at least 2-fold changed expression in SH-SY5Y cells treated with SUN N8075 at 3 μM for 3, 7 and 13 h out of the top 10% of fluorescence intensity in the non-treated control is shown in Fig. 2B and listed in Table S2. In the 320 genes, we identified the *VGF* gene as a candidate gene. The induction of *VGF* was also confirmed by real-time RT-PCR (Fig. 2C,D). SUN N8075 at a concentration of 3 μM significantly increased the *VGF* mRNA level to more than 2-fold during 13 h compared with the vehicle-treated control (Fig. 2C). Furthermore, *VGF* mRNA levels were time-dependently increased by tunicamycin, and the increase was significant for 12 h (Fig. 2D). The tunicamycin-induced *VGF* mRNA upregulation was potentiated by pretreatment with SUN N8075 at 3 μM (Fig. 2D). VGF is a neurotrophin-inducible and activity-regulated gene product expressing in the central and peripheral neurons, in which it is processed into peptides and secreted [11,25]. VGF synthesis is stimulated by brain-derived neurotrophic factor (BDNF), a critical regulator of hippocampal development and function [26,27]. However, the expression of neurotrophins, including *BDNF* and glial cell derived neurotrophic factor (*GDNF*), and neuropeptide Y (*NPY*) was not affected by SUN N8075 alone or after tunicamycin with or without SUN N8075 (Table 1). These results indicate that SUN N8075-induced VGF expression is not mediated by neurotrophins. On the other hand, SUN N8075 increased the expression of the immediate early genes (IEGs), *c-fos* and early growth response gene 1 (*EGR1*) but not cAMP response element-binding protein 1 (*CREB1*) or *JUN* (Table 1). IEGs are regulatory transcription factors, which may promote VGF expression. Alder et al. [11] reported that BDNF increases the expression of IEGs, including *c-fos* and *EGR1* at 20 min and *VGF* at 3 h, and they are blocked by mitogen-activated protein kinase kinase (MEK) inhibitor or Ca^{2+}-calmodulin-dependent protein kinase II (CaMKII) inhibitor. These findings suggest that SUN N8075 may induce VGF by regulating mitogen-activated protein kinase (MAPK) or CaMKII activity. On the other hand, almost all the 15 ER-related genes listed in Table S3 were increased after being treated with tunicamycin, but SUN N8075 did not affect the expression of ER-related genes, suggesting that SUN N8075 could not act on the UPRs themselves.

Requirement of VGF expression for the protective effects of SUN N8075 on ER stress-induced cell death

We tested the involvement of VGF in the protective effect of SUN N8075 on ER-induced cell death in SH-SY5Y cells. As shown in Fig. 3A and 3B, the *VGF* siRNA completely abolished the protective effect of SUN N8075 against tunicamycin-induced cell death. Furthermore, *VGF* siRNA aggravated tunicamycin-induced cell death compared with the control siRNA (Fig. 3B), suggesting that endogenous VGF protects cells under ER stress. In this condition, *VGF* siRNA decreased the *VGF* mRNA to 60% of the control (Fig. 3C). On the other hand, overexpression of VGF transiently transfected VGF plasmid vector inhibited cell death induced by tunicamycin compared with the empty vector-transfected control (Fig. 3D,E). These results strongly suggest that the protective effect of SUN N8075 on tunicamycin-induced cell death is mediated by the expression of endogenous VGF. Furthermore, this is the first report to demonstrate that VGF overexpression protects against ER stress-induced cell death.

SUN N8075 activates cell survival signals

VGF is upregulated by BDNF through extracellular signal-regulated protein kinase (ERK)-dependent phosphorylation of the nuclear transcription factor cAMP-response element binding protein 1 (CREB1) in primary cultures of hippocampal neurons [11]. Furthermore, BDNF protects neurons against apoptotic cell death through MEK/ERK and phosphatidylinositol 3-kinase (PI3K)/Akt pathways [28]. Activations of endogenous Akt and MEK/ERK also control cell survival during ER stress by directly counteracting ER stress [29]. Here we measured the phosphorylation levels of Akt (p-Akt) and ERK1/2 (p-ERK1/2) after SUN N8075 treatment or after tunicamycin treatment with or without SUN N8075. SUN N8075 increased p-Akt levels in a time- and

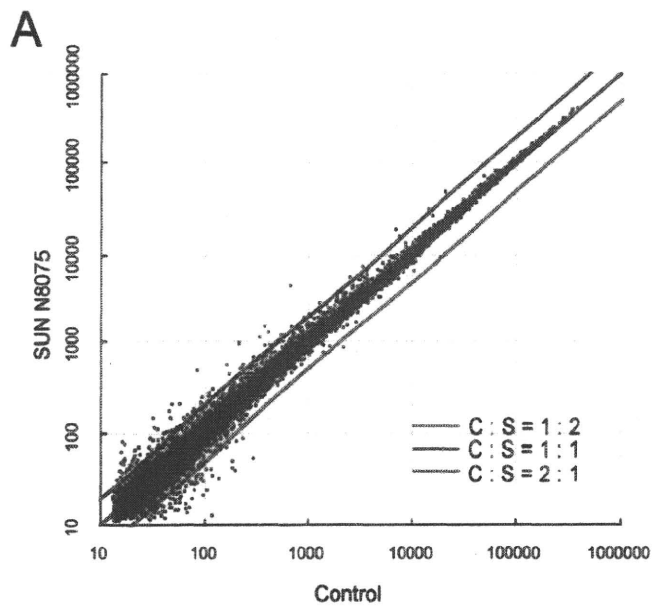
A
SUN N8075
Control
C : S = 1 : 2
C : S = 1 : 1
C : S = 2 : 1

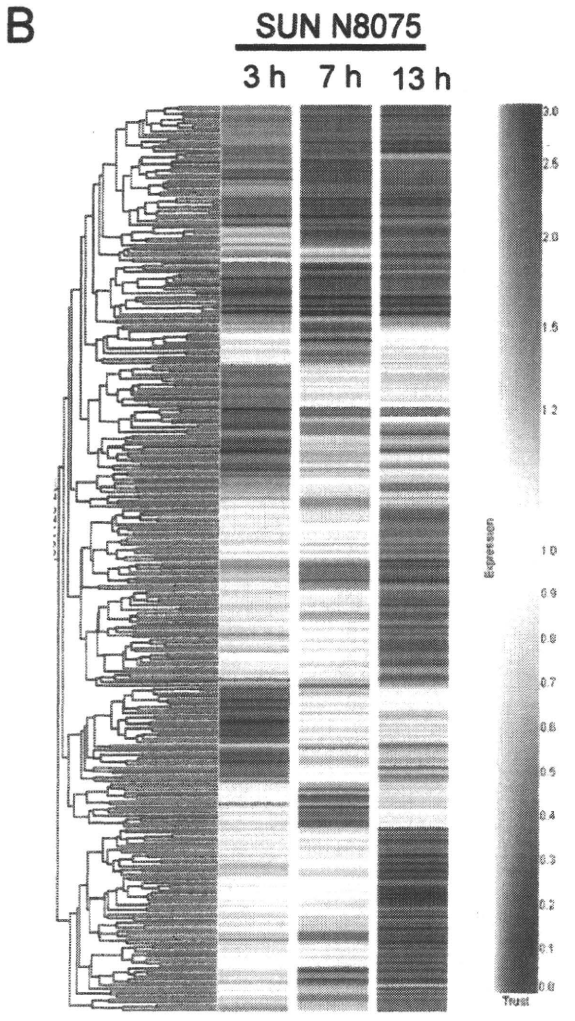
B
SUN N8075
3 h
7 h
13 h
Expression
Trust

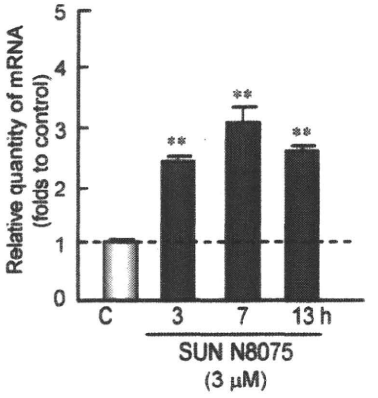
C
Relative quantity of mRNA
(folds to control)
C
3
7
13 h
SUN N8075
(3 μM)

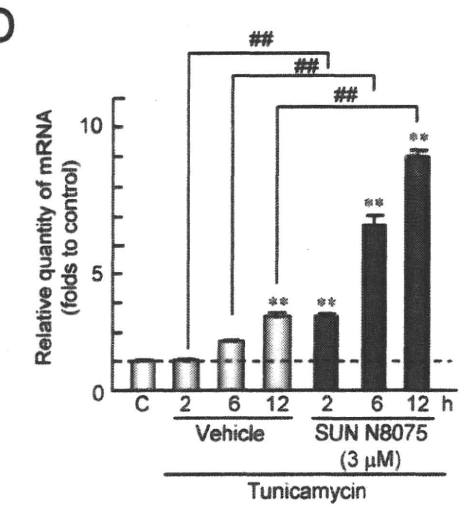
D
Relative quantity of mRNA
(folds to control)
C
2
6
12
2
6
12 h
Vehicle
SUN N8075
(3 μM)
Tunicamycin

Figure 2. Changes in the gene expression of SH-SY5Y cells after SUN N8075 treatment. (A) Representative scatter plot comparison in gene expression with DNA microarray between SUN N8075 and vehicle control treatments at 7 h. (B) Heat map representation of hierarchical clustering of 320 genes with at least 2-fold changed expression in SH-SY5Y cells treated with 3 μM of SUN N8075. The columns and rows represent samples from the time-course study and individual gene expression levels, respectively. Shades of red indicate elevated expression while shades of blue indicate decreased expression relative to the median (see the color scale). (C, D) Quantitative analysis of *VGF* mRNA after SUN N8075 (C), and after treatment with tunicamycin with or without SUN N8075 (D).
doi:10.1371/journal.pone.0015307.g002

concentration-dependent manner (Fig. S5A,B). In contrast, tunicamycin treatment for 24 h slightly reduced both pAkt and p-ERK1/2 (Fig. S5C,D). SUN N8075 inhibited the dephosphorylations of p-Akt and p-ERK1/2 at 24 h after treatment with tunicamycin (Fig. S5C,D). ER stress activates survival signals such as PI3K/Akt and MEK/ERK pathways in parallel with the UPR. Hu et al. [29] reported that Akt and ERK are activated for up to 4 h after tunicamycin or thapsigargin stimulation, and their activation is eliminated thereafter. Furthermore, Akt or MEK1 inhibition sensitized cells to ER stress-induced cell death [29]. In the present study, a PI3K inhibitor (LY294002; 20 μM) or MEK1/2 inhibitor (U0126; 5 μM) reduced cell viability, and sensitized cells to ER stress-induced cell death (Fig. S5E,F). Furthermore, the protective effect of SUN N8075 was attenuated by the pretreatment with a PI3K inhibitor (LY294002; 20 μM) or MEK1/2 inhibitor (U0126; 5 μM) (Fig. S5E,F). These data suggest that SUN N8075 enhances survival signals such as PI3K/Akt and MEK/ERK pathways. As mentioned above, VGF may be upregulated by ERK-dependent phosphorylation of CREB1 or induction of other IEGs including *c-fos* and *EGR1* after SUN N8075.

Motor dysfunction and survival in ALS models

To confirm the effects of SUN N8075 on motor dysfunction and the survival of the familiar ALS model, we used two types of transgenic animals overexpressing mutated human SOD1 genes: transgenic mice overexpressing mutated (glycine to alanine in position 93) human SOD1 (G93A) [16] and transgenic rats overexpressing mutated (histidine to arginine in position 46) human SOD1 (H46R) [17]. Treatment with SUN N8075 was started when the G93A mice were 10 weeks old and the H46R rats were 15 weeks old before each disease onset.

In the G93A mice, motor performance was tested by a rotarod test (Fig. 4A). Vehicle-treated G93A mice began to show a decline in motor performance around the age of 100 days that continued to be gradually impaired thereafter; the mice were unable to perform the test around the age of 130 days. Treatment with SUN N8075 (30 mg/kg/day s.c.) prolonged the decline of latency to fall off the rod. Kaplan–Meier life curves suggested that treatment with SUN N8075 prolonged disease onset ($p = 0.024$) and survival ($p = 0.0351$) in the G93A mice (Fig. 4B,C). In the G93A model mice, the mean survival days of the vehicle-treated and the SUN N8075-treated mice were 122.8 ± 4.0 ($n = 12$) and 136.2 ± 3.4 ($n = 12$), respectively (Fig. 4C). Treatment with SUN N8075 significantly prolonged the mean lifespan by 10.9% ($p = 0.0178$) in the G93A mice compared with that in the vehicle-treated G93A mice. On the other hand, there was no significant difference in the course of body weight between the SUN N8075-treated and the vehicle-treated G93A mice (Fig. S6A).

Next, we used SOD1 H46R mutant rats as other types of familial ALS models to evaluate the effects of SUN N8075 on motor dysfunction and survival. H46R is one of 119 known SOD1 mutations that cause familial ALS, and H46R rats are characterized by initial muscle weakness and atrophy in the legs, very long clinical courses and include many neuropil aggregates that lack vacuoles [30]. In the H46R rats, the motor score was determined by a 5-point motor score system (Fig. 4D). The vehicle-treated H46R rats began to show a decline in motor performance around the age of 170 days that continued to be gradually impaired thereafter; the mice were unable to perform the test around the age of 220 days. Treatment with SUN N8075 (10 mg/kg/day s.c.) prolonged the decline of the motor score. Kaplan–Meier life curves suggested that treatment with SUN N8075 prolonged disease onset ($p = 0.012$) and survival ($p = 0.011$) in H46 rats

Table 1. Gene expression of *VGF*, neurotrophins and gene transcription factors in SH-SY5Y cells after SUN N8075 and during ER stress with or without SUN N8075.

		Fold change (vs. control)						
					6 h after Tm		12 h after Tm	
Gene	Genbank	Time after SUN N8075			Vehicle	SUN	Vehicle	SUN
Symbol	Accession	3 h	7 h	13 h	7 h	7 h	13 h	13 h
VGF	NM_003378	1.25	1.94	2.21	1.12	2.72	2.43	6.78
NPY	NM_000905	1.22	1.43	1.64	0.57	0.84	0.82	1.20
BDNF	NM_170735	0.82	0.85	0.94	0.86	0.69	0.58	0.58
GDNF	AJ001898	1.12	1.04	0.93	0.91	0.84	0.91	0.89
FOS	NM_005252	2.42	1.67	1.76	1.01	3.29	1.14	1.86
EGR1	NM_001964	2.75	1.93	1.73	2.61	11.19	1.15	2.63
JUN	NM_002228	0.72	1.00	0.94	2.63	2.26	2.02	1.86
CREB1	NM_134442	1.08	1.09	1.02	1.04	1.21	0.87	0.95

SUN N8075 at a concentration of 3 μM was treated for 3, 7 or 13 h. One hour before tunicamycin treatment, SUN N8075 was treated, then tunicamycin was treated for 6 (7 h after SUN) or 12 h (13 h after SUN). *VGF*: VGF nerve growth factor inducible, *NPY*: Neuropeptide Y, *BDNF*: Brain-derived neurotrophic factor, *GDNF*: Glial cell derived neurotrophic factor, FOS: c-fos proto-oncogene, *EGR1*: Early growth response protein 1, *JUN*: Jun oncogene, *CREB1*: cAMP responsive element binding protein 1, SUN: SUN N8075, Tm: tunicamycin.
doi:10.1371/journal.pone.0015307.t001